Molecular Biology of the Cell
Vol. 12, 629–644, March 2001

Signaling Mediated by the Cytosolic Domain of Peptidylglycine α-Amidating Monooxygenase

M. Rashidul Alam,* Tami C. Steveson, Richard C. Johnson,† Nils Bäck,‡ Benjamin Abraham,§ Richard E. Mains, and Betty A. Eipper‖

Department of Neuroscience, University of Connecticut Health Center, Farmington, Connecticut 06030-3401

Submitted May 2, 2000; Revised December 20, 2000; Accepted January 4, 2001
Monitoring Editor: Howard Riezman

The luminal domains of membrane peptidylglycine α-amidating monooxygenase (PAM) are essential for peptide α-amidation, and the cytosolic domain (CD) is essential for trafficking. Overexpression of membrane PAM in corticotrope tumor cells reorganizes the actin cytoskeleton, shifts endogenous adrenocorticotropic hormone (ACTH) from mature granules localized at the tips of processes to the TGN region, and blocks regulated secretion. PAM-CD interactor proteins include a protein kinase that phosphorylates PAM (P-CIP2) and Kalirin, a Rho family GDP/GTP exchange factor. We engineered a PAM protein unable to interact with either P-CIP2 or Kalirin (PAM-1/K919R), along with PAM proteins able to interact with Kalirin but not with P-CIP2. AtT-20 cells expressing PAM-1/K919R produce fully active membrane enzyme but still exhibit regulated secretion, with ACTH-containing granules localized to process tips. Immunoelectron microscopy demonstrates accumulation of PAM and ACTH in tubular structures at the *trans* side of the Golgi in AtT-20 cells expressing PAM-1 but not in AtT-20 cells expressing PAM-1/K919R. The ability of PAM to interact with P-CIP2 is critical to its ability to block exit from the Golgi and affect regulated secretion. Consistent with this, mutation of its P-CIP2 phosphorylation site alters the ability of PAM to affect regulated secretion.

INTRODUCTION

AtT-20 corticotrope tumor cells have long served as a reliable model system for studying the biosynthesis, storage, and regulated secretion of pituitary peptide hormones (Mains and Eipper, 1978; Moore and Kelly, 1986; Tooze and Tooze, 1986). Cleavage of endogenous pro-opiomelanocortin (POMC) by PC1 (PC1) and carboxypeptidase E yields both adrenocorticotropic hormone (ACTH) and β-lipotropin (Fricker and Devi, 1993; Zhou *et al.*, 1993). Production of other POMC peptides requires the action of peptidylglycine α-amidating monooxygenase (PAM) (Eipper *et al.*, 1986). Although levels of PAM in AtT-20 cells are 20-fold lower than in the anterior pituitary, complete amidation of POMC-derived products occurs (Eipper *et al.*, 1986).

PAM is one of the few peptide-processing enzymes that spans the secretory granule membrane. The fact that its luminal, catalytic domains are pH sensitive and are further activated on cleavage from the membrane (Husten and Eipper, 1991; Husten *et al.*, 1993) raised the possibility that PAM might play a role in signaling luminal conditions to the cytosolic machinery involved in secretory granule formation. This type of signaling is essential in communicating information about events occurring in the lumen of the endoplasmic reticulum to cytosolic proteins (Pahl and Baeuerle, 1997; Shamu, 1997; Brown and Goldstein, 1998), as well as in cargo selection during vesicle budding (Kuehn and Herrmann, 1998).

We were surprised to find that expression of exogenous PAM in AtT-20 cells at levels equivalent to those in the anterior pituitary blocked the regulated secretion of ACTH,

‖ Corresponding author. E-mail: eipper@uchc.edu.the Present addresses: * Laboratory of Oral Medicine, Building 30, Room 122, NIDCR, National Institutes of Health, 30 Convent Drive, Bethesda, MD 20892; † Department of Neurosciences, Johns Hopkins University School of Medicine, 725 North Wolfe Street, Baltimore, MD 21205; § Department of Neurology, Johns Hopkins University School of Medicine, 725 North Wolfe Street, Baltimore, MD 21205; ‡Department of Anatomy, Institute of Biomedicine and Department of Basic Veterinary Sciences, University of Helsinki, Helsinki, Finland 00014.

Abbreviations used: ACTH, adrenocorticotropic hormone; DC, COOH-terminal domain of PAM; CHO, Chinese hamster ovary; FITC, fluorescein isothiocyanate; Gal4(DB), Gal4 DNA-binding domain; Gal4(TA), Gal4 transactivator domain; GST, glutathione *S*-transferase; PAL, peptidylglycine α-amidating lysase; PAM, peptidylglycine α-amidating monooxygenase (E.C. 1.14.17.3); PC1, prohormone convertase 1; P-CIP, PAM-COOH-terminal interactor protein; PCR, polymerase chain reaction; PHM, peptidylglycine α-hydroxylating mono-oxygenase; POMC, proopiomelanocortin; TGN, *trans*-Golgi network.

relocated ACTH-containing granules from the tips of cellular processes to the *trans*-Golgi network (TGN) area, and altered the distribution of filamentous actin (Ciccotosto *et al.*, 1999; Mains *et al.*, 1999). By examining AtT-20 cells expressing PAM under control of an inducible promoter and after infection with adenovirus encoding PAM, we established a causal relationship between PAM overexpression and impaired operation of the regulated secretory pathway (Ciccotosto *et al.*, 1999). Knowing that overexpression of PAM caused these changes, we next sought to distinguish between two possibilities: first, high levels of membrane protein expression might nonspecifically inhibit protein trafficking; second, high levels of PAM expression might selectively interfere with a normal trafficking step. To distinguish between these two possibilities, we undertook construction of point mutants of PAM that could not interact with known cytosolic domain interactors. Elimination of this paradoxical effect of PAM by mutation would suggest selective interference with a normal trafficking step.

We knew from our earlier studies that the trafficking of membrane PAM shares many features with other type 1 membrane proteins (Milgram *et al.*, 1993, 1994b). The unique aspect of PAM trafficking is its entry into secretory granules, where it can undergo endoproteolytic cleavage by the same enzymes that cleave POMC (Milgram *et al.*, 1992; Milgram and Mains, 1994). The small amount of PAM that reaches the plasma membrane rapidly undergoes endocytosis, returning to the TGN region (Milgram *et al.*, 1996). The cytosolic domain of PAM contains a Tyr-based internalization motif, and endocytosis is affected by phosphorylation at multiple sites (Milgram *et al.*, 1993; Yun *et al.*, 1995; Steveson *et al.*, 1999). When proteins capable of interacting with the cytosolic domain of PAM were sought, we anticipated identifying coat proteins, adaptor proteins, components of the SNARE complex, Rab proteins, and motor proteins. Instead, we found P-CIP2 (PAM-cytosolic domain interactor protein 2), a protein kinase selective for the cytosolic domain of PAM (Caldwell *et al.*, 1999), Kalirin, a GDP/GTP exchange factor for Rac1 (Alam *et al.*, 1996, 1997), and P-CIP1, a novel protein associated with endosomes (Chen *et al.*, 1998).

In this study, we identify a mutation in PAM that eliminates the binding of P-CIP2 and Kalirin without affecting the activity of the catalytic domains or dramatically altering the endoproteolytic cleavage or endocytosis of PAM. Expressed at the same level as PAM-1, this mutant protein (Lys^{919} to Arg; PAM-1/K919R) does not impair the function of the regulated secretory pathway, demonstrating that this is not a nonspecific overexpression phenotype. Analysis of additional PAM mutants identifies the interaction with P-CIP2 as essential to this response. Consistent with this conclusion, mutation of the P-CIP2 phosphorylation site in PAM to Asp also eliminates the ability of PAM to disrupt regulated secretion. Immunoelectron microscopy indicates that overexpression of PAM, but not PAM-1/K919R, results in an accumulation of PAM and ACTH in tubulovesicular structures in the TGN area. We suggest that P-CIP2, through its interaction with and phosphorylation of the cytosolic domain of PAM, plays a key role in the formation of immature secretory granules from *trans*-Golgi cisternae.

MATERIALS AND METHODS

PAM-Cytosolic Domain (CD) Mutagenesis and Yeast Two-Hybrid Analysis

Saccharomyces cerevisiae reporter strains HF7c (Feilotter *et al.*, 1994) and Y190 (Harper *et al.*, 1993) were used for yeast two-hybrid analysis. The sequence of a truncated form of PAM-CD (rPAM[890–961]; Alam *et al.*, 1996) was used. A set of primers (sense, 5′-AGGTCGACCCGGTGGAAAAAATCAAG-3′; and antisense, 5′-GGACTAGTAAGACTCAGTTCCGTCGTC-3′), complementary to the cDNA at both the 5′ and 3′ ends of the truncated PAM-CD, was used to perform low-fidelity polymerase chain reaction (PCR) random mutagenesis (Leung *et al.*, 1989). Initially, an aliquot of the 225-base pair (bp) PCR product was subcloned into pBluescript (Stratagene, La Jolla, CA), and DNA sequence analysis of a representative sample of clones determined that the frequency of point mutations averaged one per truncated CD. The mutated PCR products were digested with *Sal*I and *Spe*I and ligated downstream of *Gal4DB* in the yeast two-hybrid vector pPC97 (Chevray and Nathans, 1992). MAX Efficiency *Escherichia coli* strain DH5α (BRL, Rockville, MD) was used for transformation of the ligation reaction, and the mutagenized pPC97.CD library was prepared by pooling all transformants.

Library DNA (0.9 μg) was used to transform the HF7c strain of *S. cerevisiae* previously transformed with pPC86.I-10 (the original Kalirin[447–1124] interactor domain; Alam *et al.*, 1997) and selection for double transformants was performed using a synthetic dextrose medium deficient in Trp and Leu. Independent colonies (1440) were picked and challenged for growth on medium deficient in Trp, Leu, and His plus 15 mM 3-amino-1,2,4-triazole (Sigma, St. Louis, MO) for 3 d at 30°C, and colonies having poor or no growth were identified. To eliminate frameshift and nonsense mutants, extracts of all 133 poorly growing clones were subjected to Western blot analysis; only the 26 expressing full-length Gal4DB:CD fusion protein were pursued. Plasmid DNAs rescued from these colonies were sequenced, yielding 24 independent inserts bearing from one to five point mutations. Twenty-nine of the 71 positions in truncated PAM-CD were mutated in the clones tested. The PAM-CD mutants were tested for their ability to interact with Kalirin(447–1124) and P-CIP2(28–419) using the liquid-phase β-galactosidase assay: with Kalirin, five exhibited $<$10% of the activity of wild-type PAM-CD; with P-CIP2, 12 showed $<$1% of the activity of wild-type PAM-CD.

Because most of these isolated truncated CD mutants harbored mutations at multiple sites, a second generation of mutant truncated CDs with single-point mutations were produced using a cut-and-paste strategy with the appropriate restriction enzymes. Each mutant pPC97.CD, along with pPC86.I-10 DNA, was transformed into yeast strain Y190 so that β-galactosidase assays could be used to quantify the strength of the CD interaction with I-10 (Ratovitski *et al.*, 1999). The double transformants were grown and assayed for β-galactosidase activity following the liquid assay protocol from Clontech (Palo Alto, CA). Using similar methods, we also tested the set of CD mutant vectors against pPC86.I-2, the original P-CIP2 interactor domain (Alam *et al.*, 1996).

In Vitro Binding Assay

Expression vectors pGEX-3X and pGEX-4T-2 (Pharmacia, Piscataway, NJ) were used to produce glutathione *S*-transferase (GST) fusion proteins (Alam *et al.*, 1996). All fusion proteins were purified following the Pharmacia protocol and dialyzed against phosphate-buffered saline before storage at −80°C. Glutathione-Sepharose beads with bound fusion proteins were prepared before each binding assay. Chinese hamster ovary (CHO) cells expressing *myc*.Kalirin (Mains *et al.*, 1999) were extracted in binding buffer (20 mM potassium-HEPES, 150 mM potassium acetate, 1% Triton X-100 containing protease inhibitors), and 300 μg of solubilized total CHO cell protein were mixed with 10 μg of GST or GST-CD fusion protein bound to ~20 μl of glutathione-Sepharose beads. The mix-

ture was incubated at 4°C for 3 h with continuous shaking. The beads were separated from the cell extract and washed three times with binding buffer. Both beads and the unbound cell extracts were boiled into SDS-PAGE loading buffer, and 25% of each sample was applied to a 6% polyacrylamide gel; the proteins were transferred to polyvinylidene difluoride membranes and subjected to Western blot analysis (Milgram *et al.*, 1992).

Antibodies

The rabbit antisera used in this study were JH629, exon 16 (rat PAM-1[393–498]; Mains *et al.*, 1999); JH1761, peptidylglycine α-hydroxylating mono-oxygenase (PHM) domain (rat PAM[37–382]; Milgram *et al.*, 1992); JH888, PC1 (Zhou and Mains, 1994); JH93, NH_2-terminal end of ACTH, capable of binding intact POMC (Zhou *et al.*, 1993); Kathy, specific for the COOH terminus of ACTH (Schnabel *et al.*, 1989); and JH2582, spectrin repeats 4 to 7 of Kalirin (Mains *et al.*, 1999). Monoclonal antibodies used were cation-independent mannose 6-phosphate receptor, kindly provided by Dr. Suzanne Pfeffer (Dintzis *et al.*, 1994); 1D4B (Developmental Studies Hybridoma Bank, Baltimore, MD), directed against lysosome-associated membrane protein 1 (Hughes and August, 1981); γ-adaptin (Transduction Labs, Lexington, KY); and ACTH (Novocastra Laboratories, Newcastle upon Tyne, UK). It is apparent from analysis of the PAM-CD mutants that monoclonal antibody 6E6 (Milgram *et al.*, 1997) exhibits specificity for the region around Phe^{941}.

Immunofluorescent Staining of Cells

Cells plated on poly-L-lysine-coated glass chamber slides were fixed with ice cold methanol or warm 4% paraformaldehyde and stained as described previously (Milgram *et al.*, 1996, 1997). Double staining was performed using rabbit polyclonal and mouse monoclonal antibodies. The rabbit polyclonal antibodies were visualized with fluorescein isothiocyanate (FITC)-tagged goat anti-rabbit $F(ab')_2$ immunoglobulin G(H + L) (Caltag Laboratories, Burlingame, CA), and the monoclonal antibodies were visualized with Cy^3-tagged AffiniPure donkey anti-mouse IgG(H + L) (Jackson ImmunoResearch Laboratories, West Grove, PA). Actin filaments were visualized after the cells were fixed with paraformaldehyde (3.7%) for 10 min and incubated with FITC-phalloidin (0.125–0.5 μg/ml) for 30 min. Cells were viewed and photographed as described earlier (Milgram *et al.*, 1996, 1997). To evaluate trafficking in the endocytic pathway, antibody uptake experiments were conducted as described previously (Milgram and Mains, 1994).

Immunoelectron Microscopy

Cells were fixed with 4% paraformaldehyde, 0.05% glutaraldehyde, and 2% sucrose in 0.1 M phosphate buffer, pH 7.2, for 1 h, postfixed with 0.25% tannic acid for 1 h, scraped, and pelleted in a fibrinogen-thrombin clot (Raska *et al.*, 1998). Cryosectioning and immunogold labeling were performed as described before (Griffiths, 1993). Polyvinylpyrrolidone/sucrose-infiltrated specimens were sectioned at −100°C, and the sections were incubated with PAM antibody JH629 (1:200) for 1 h. Secondary antibody (Protein A–10-nm gold; University of Utrecht, Utrecht, The Netherlands) was applied for 1 h, and sections were embedded in uranyl acetate-methyl cellulose (Griffiths, 1993). For double staining, PAM-stained sections were fixed with 4% formaldehyde, 1% glutaraldehyde in phosphate-buffered saline for 10 min, rinsed, and incubated with ACTH antibody Kathy for 1 h, followed by secondary antibody (protein A–15-nm gold). Controls omitted primary antibodies. Conventional sections were made as described previously (Mains *et al.*, 1999).

Biosynthetic Labeling and Immunoprecipitation

Cells were plated on 15-mm culture dishes coated with poly-L-lysine and grown to 70–90% confluency before biosynthetic labeling. Cells were incubated in methionine-free complete serum-free medium for 10 min and then with the same medium containing 0.8 mCi/ml [^{35}S]Met (Amersham, Arlington Heights, IL) for 15 min followed by a chase in complete serum-free medium. Chase media were centrifuged and cells were extracted in TMT (10 mM Na TES, pH 7.5, 20 mM mannitol, 1% Triton X-100, plus protease inhibitor cocktail; Milgram *et al.*, 1992). Immunoprecipitation of PAM, ACTH, and PC1 was performed using antisera JH1761, JH93, and JH888, respectively. Immunoprecipitated proteins were resolved by SDS-PAGE and visualized by fluorography. For quantification, autoradiograms were densitized using National Institutes of Health Image (Milgram *et al.*, 1993).

Cells and Secretion Studies

All cells were maintained in DMEM/F-12 containing 10% fetal bovine serum (Hyclone, Logan, UT) and 10% NuSerum (Collaborative Research, Bedford, MA) and passaged weekly. CHO cells stably expressing *myc*.Kalirin (Mains *et al.*, 1999) were maintained with medium containing hygromycin (200 U/ml), and AtT-20 cells stably expressing PAM-1 (Milgram *et al.*, 1992) and several PAM-1 mutants were maintained with G418 (0.5 mg/ml). To construct cDNAs encoding the PAM-1 mutants, the ~0.26- kilobase fragment of the mutant CD was ligated into pCI.neo.PAM-1 prepared with *Xho*I-*Xba*I. Clonal AtT-20 cell lines expressing mutant PAM-1 (more than five lines from three separate transfections) were selected using G418 and screened by immunostaining, enzyme assay and Western blot (Milgram *et al.*, 1994a). The sequence of the expressed PAM-1/K919R mRNA was verified by preparing cDNA using reverse transcriptase-PCR and sequencing the cDNA to confirm the presence of the mutation.

To study secretion of PHM, ACTH, and PC1 from nontransfected, PAM-1, and PAM-1 mutant-expressing AtT-20 cells, duplicate wells of cells were plated on poly-L-lysine-coated plastic plates. Cells were equilibrated for three 30-min periods with basal release medium (DMEM-F12-Air with 2 mg/ml fatty-acid free bovine serum albumin, 0.1 mg/ml lima bean trypsin inhibitor, 1 μg/ml insulin, 0.1 μg/ml transferrin); this medium was discarded (Ratovitski *et al.*, 1999). Basal secretion was measured in two subsequent 30-min collections; stimulated secretion was measured after the addition of 1 mM $BaCl_2$, an effective secretagogue for mature granules (El Meskini *et al.*, 2000), which has been shown to produce sustained secretion mimicking natural secretagogues such as corticotropin releasing hormone (Mains and Eipper, 1981). Harvested medium was centrifuged to remove nonadherent cells, and protease inhibitors were added before storage at −80°C. Cells were extracted with 20 mM sodium TES (*N*-Tris(hydroxymethyl)methyl-2-aminoethanesulfonic acid), 10 mM mannitol, pH 7.0, containing 1% Triton X-100 for measurement of PHM activity or with 5 N acetic acid for measurement of immunoactive ACTH (Ratovitski *et al.*, 1999). Immunoactive ACTH was detected using COOH-terminal ACTH antiserum Kathy, which reacts equally with ACTH biosynthetic intermediate and ACTH but does not detect intact POMC (Schnabel *et al.*, 1989). Media samples were assayed for PHM and peptidylglycine α-amidating lyase (PAL) activity and subjected to Western blot analysis.

P-CIP2 Coimmunoprecipitation

Confluent 100-mm dishes of cells were rinsed with serum-free medium for 5 min, placed on ice, and covered with 2 ml of 20 mM piperazine-*N*,*N*′-bis(2-ethanesulfonic acid), pH 6.8, 2 mM Na_2EDTA, 50 mM NaF, 10 mM $Na_4P_20_7$, 1 mM Na_3VO_4, 1% Triton X-100, and 0.3 mM PMSF and extracted for 15 min (Ratovitski *et al.*, 1999). Cells were scraped from the plate and centrifuged at 75,000 × *g* for 20 min. Aliquots of the supernatant (200 μl) were subjected to immunoprecipitation with rabbit polyclonal antiserum to P-CIP2 (10 μl; Ab1998; Alam *et al.*, 1996). After incubation at 4°C for 1.5 h, samples were centrifuged, incubated with protein A-Sepharose beads for 1 h at 4°C, washed twice in extraction buffer, and eluted

by boiling into SDS sample buffer. Controls included blocking by addition of recombinant GST–P-CIP2 and analysis of nontransfected cells.

RESULTS

Mutagenesis of the CD-PAM Identifies Lys^{919} as Critical for Interaction with Kalirin and P-CIP2 in the Yeast Two-Hybrid System

To identify residues in the CD-PAM that are critical to its ability to interact with Kalirin and P-CIP2, we used low-fidelity PCR mutagenesis. We used the liquid-phase β-galactosidase assay to assess the ability of each mutant PAM-CD/Gal4 DNA-binding domain (Gal4(DB)) fusion protein to interact with the Kalirin and P-CIP2 Gal4 transactivator domain (Gal4(TA)) fusion proteins originally identified in our yeast two-hybrid screen (Alam *et al.*, 1996). Kalirin(447–1124) is part of the spectrin repeat-like region of Kalirin, and P-CIP2(28–419) includes all but the first 27 residues of P-CIP2. We recovered mutations in about one-half of the residues of PAM-CD and identified 11 sites as potentially important, constructing PAM-CD/Gal4(DB) fusion proteins bearing single-point mutations at these sites (Table 1). Based on previous work demonstrating its role in internalization from the plasma membrane, we also screened a fusion protein bearing the Y936A mutation (Milgram *et al.*, 1996). Expression of these mutant PAM-CD/Gal4(DB) fusion proteins in yeast was verified by Western blot analysis.

When tested for their ability to interact with Kalirin/Gal4(TA), PAM-CD/Gal4(DB) fusion proteins bearing the K919R mutation or the Y936A mutation showed a dramatically diminished interaction (Table 1). Mutations at 28 other sites failed to affect significantly the interaction of PAM-CD with Kalirin. Although Y^{936} was previously identified as a key determinant in the internalization of PAM, a role for K^{919} was not anticipated based on previous studies.

The set of mutant PAM-CD/Gal4(DB) fusion proteins were also tested for their ability to interact with P-CIP2/Gal4(TA) (Table 1). Analysis of the PAM-CD mutants identified four single-site mutations that completely eliminated interaction with P-CIP2; mutations at the remaining sites had no significant effect. The K919R mutation is the only single amino acid change that eliminated the ability of PAM-CD/Gal4(DB) to interact with both Kalirin/Gal4(TA) and P-CIP2/Gal4(TA). Mutation of any one of three closely spaced hydrophobic residues (L926Q, F929S, and F930S) independently resulted in complete loss of CD interaction with P-CIP2 (Table 1). The interaction of PAM-CD with P-CIP2 was not altered by mutation of Y^{936}.

Table 1. Analysis of mutant PAM-CD/Gal4(DB) fusion proteins

PAM-CD mutation	β-Galactosidase Activity Kalirin(447–1124), % WT	β-Galactosidase activity P-CIP2(28–419), % WT
Wild Type, WT	100	100
F898L	123	87
H901R	324	135
D902G	NE	NE
S907P	NE	NE
S908R	NE	NE
R911G	57	42
V912D	144	108
F916S	87	132
K919R	1	0
L924I	NE	NE
N925S	190	119
L926Q	90	0
F929S	53	0
F930S	44	0
S932R	NE	NE
K934I	NE	NE
Y936A	10	73
S937A	NE	NE
K939Q	NE	NE
F941S	101	59
V944A	NE	NE
S949A	NE	NE
D950G	NE	NE
Q951P	NE	NE
E952V	NE	NE
D954G	NE	NE
E955G	NE	NE
D956N	NE	NE
T959stop	NE	NE
S961A	NE	NE

The truncated CD-PAM (PAM[890–961]) was subjected to mutagenesis as described in MATERIALS AND METHODS. Analysis of the first set of mutant PAM-CD/Gal4(DB) fusion proteins identified sites at which mutation failed to affect interaction with Kalirin(447–1124)/Gal4(TA) or P-CIP2(28–419)/Gal4(TA). Sites identified as nonessential in this first screen are indicated by NE and were not studied further. Sites of potential importance were studied as single-site mutant PAM-CD/Gal4(DB) fusion proteins; the strength of each interaction with Kalirin/Gal4(TA) and P-CIP2/Gal4(TA) was quantified using the liquid-phase β-galactosidase assay. Wild-type PAM-CD/Gal4(DB) was taken as 100%, and data are the means from three independent assays with SD all <15% of the mean. Levels of mutant PAM-CD/Gal4(DB) fusion protein expression were comparable as judged by Western blot using polyclonal and monoclonal PAM-CD antibodies; monoclonal antibody 6E6 failed to cross-react with PAM-CD(F941S)/Gal4(DB).

Mutation of Lys^{919} to Arg Eliminates Interaction of PAM with Kalirin and with P-CIP2

Because PAM-CD(K919R)/Gal4DB was the only mutant fusion protein that failed to interact with both P-CIP2 and Kalirin in the yeast two-hybrid assay, we initially focused our attention on this particular PAM-CD mutant. We tested mutant PAM-CD interactions with full-length Kalirin in test tube binding studies. PAM-CD/GST fusion proteins with wild-type CD, CD bearing the Lys^{919} to Arg mutation (K919R), or a truncated CD (936 stop, 936s) were expressed and bound to glutathione-Sepharose beads; Coomassie staining confirmed loading of similar amounts of GST control and each PAM-CD/GST fusion protein (Figure 1A, Bottom). PAM truncated at residue 936 accumulates on the cell surface, indicating loss of major routing determinants (Milgram *et al.*, 1996).

To evaluate interactions with Kalirin, GST fusion proteins bound to beads were incubated with extracts of CHO cells stably expressing full-length *myc*.Kalirin (Mains *et al.*, 1999; Figure 1A, Top). As expected, Kalirin binds to beads loaded with GST-CD but not to control GST beads. In agreement

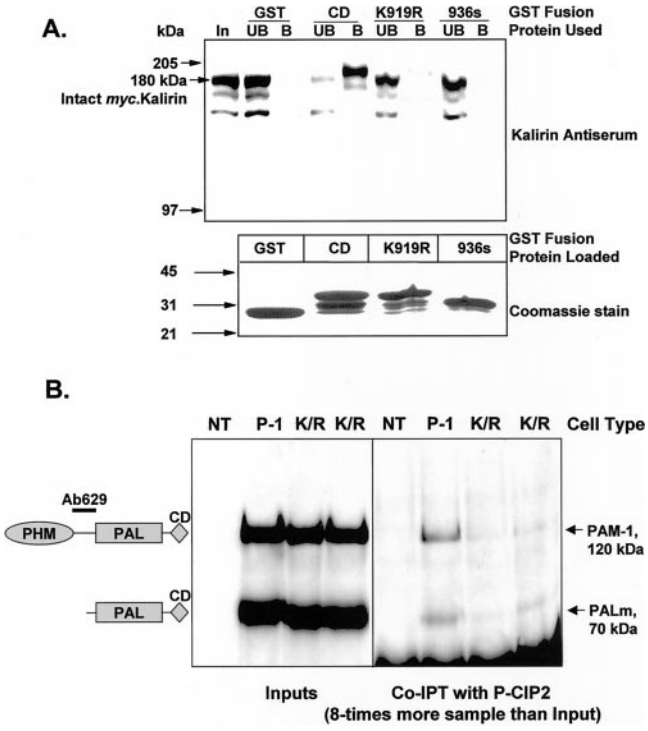

Figure 1. Verification that mutant PAM-CDs fail to interact with Kalirin or P-CIP2. (A) Kalirin binding to mutant PAM-CD/GST fusion proteins: CHO cells stably expressing *myc*.Kalirin were extracted and used as the source of Kalirin (Mains *et al.*, 1999). Purified GST, PAM-CD/GST, PAM-CD(K919R)/GST, and PAM-CD936s/GST were each bound to glutathione-Sepharose as described in MATERIALS AND METHODS. The resins were then incubated with CHO cell extract (300 μg of protein) to allow Kalirin binding; unbound proteins were collected by pelleting the resins. The resins were washed, and bound proteins were eluted by boiling in SDS-PAGE sample buffer. Top, comparable aliquots of Kalirin-containing cell extract (In), unbound (UB), and bound (B) fractions were subjected to Western blot analysis using antibody to Kalirin. Bottom, GST-fusion proteins eluted from equal aliquots of the different resins were fractionated by SDS-PAGE and visualized with Coomassie brilliant blue after transfer to a membrane. (B) P-CIP2 binding to mutant PAM-1: nontransfected (NT) AtT-20 cells and AtT-20 cells expressing PAM-1 or PAM-1/K919R (two clones, K/R) were extracted with detergent; Western blot analysis using a PAM antiserum (Ab629) demonstrated equal amounts of PAM protein in the transfected cells (Inputs). Aliquots of each extract were immunoprecipitated with antibody to P-CIP2, fractionated by SDS-PAGE, and visualized with the same PAM antibody (CoIPT with P-CIP2); eightfold more sample was used for coimmunoprecipitation than for analysis of the input. The experiment was repeated three times with the same result; the CoIPT was blocked with excess GST/P-CIP2. The diagram to the left identifies the different PAM proteins and the specificity of Ab629.

with the yeast two-hybrid analyses, beads loaded with GST-CD/K919R were unable to bind Kalirin. Despite the presence of Lys^{919}, beads loaded with GST-CD936s did not bind Kalirin (Figure 1A). It is not clear why Western blot analysis reveals a heterogeneous collection of Kalirin proteins in stably transfected CHO cells; pulse labeling of the CHO cells yielded a single immunoprecipitable Kalirin protein of 180 kDa (Alam *et al.*, 1997).

PAM-1 bearing the K919R mutation (PAM-1/K919R) was stably expressed in AtT-20 cells to evaluate the effect of this mutation on the ability of full-length PAM-1 to interact with P-CIP2, which is expressed in AtT-20 cells (Alam *et al.*, 1996). Coimmunoprecipitation was used to compare the interaction of P-CIP2 with PAM-1 and PAM-1/K919R (Figure 1B). Input samples contained intact PAM-1 (120 kDa) as well as its normal 70-kDa cleavage product, membrane PAL (Figure 1B; PALm); levels of endogenous PAM in nontransfected cells are too low to allow visualization under these conditions. Aliquots of cell extracts were incubated with rabbit polyclonal antiserum to P-CIP2, and antigen/antibody complexes isolated on protein A beads were fractionated by SDS-PAGE. A small but significant fraction of the PAM-1 and 70-kDa membrane PAL were recovered in the PCIP-2 immunoprecipitate. PAM-1/K919R (K/R) failed to coprecipitate with P-CIP2. This result is in agreement with the yeast two-hybrid analysis and was verified in extracts of two clones of AtT-20 cells expressing PAM-1/K919R.

PAM-1/K919R Is Not Misfolded

We used a variety of methods to determine whether mutation of Lys^{919} to Arg had a nonspecific effect on the structure of PAM-1. The PHM and PAL domains of PAM-1/K919R were both enzymatically active, with the PHM specific activity of two of the PAM-1/K919R cell lines comparable to that of cells expressing PAM-1: 8.8 $\pm$ 0.4 and 13.4 $\pm$ 3.4 pmol $\cdot$ $\mu g^{-1} \cdot h^{-1}$ for two PAM-1/K919R clones (mean $\pm$ SD); 14.8 $\pm$ 1.2 pmol $\cdot$ $\mu g^{-1} \cdot h^{-1}$ for PAM-1 cells (Milgram *et al.*, 1992, 1994b).

To determine whether the K919R mutation affected PAM metabolism, extracts of PAM-1/K919R and PAM-1 cells containing equal amounts of protein were subjected to Western blot analysis; PAM proteins were detected using antibodies to several different regions of PAM (Figure 2A). PAM proteins are subject to endoproteolytic cleavage only after they pass the site of the 20°C block and enter immature secretory granules (Milgram and Mains, 1994). Antibody to the noncatalytic exon 16 region that separates the PHM domain from the PAL domain (see Figure 1B) visualizes a doublet of monofunctional PHM as well as PALm and intact PAM-1 (Figure 2A). Antibody to PHM visualizes monofunctional PHM and intact PAM-1. Antibody to the PAM-CD visualizes PALm and intact PAM-1. With the amount of protein analyzed, endogenous PAM is undetectable. Comparable levels of expression were observed in cell lines expressing PAM-1/K919R and PAM-1. Importantly, similar cleavage patterns were observed, indicating that both proteins have similar access to secretory granule proteases.

Metabolic labeling studies were carried out to compare the kinetics of cleavage and rates of secretion of PAM-1/K919R and PAM-1 (Figure 2B). Cells were incubated in medium containing [^{35}S]Met for 15 min and either harvested immediately (pulse) or chased for 1, 2, or 4 h. After the 15-min pulse, a 117-kDa PAM protein was observed in both cell types. During the first 1 h of chase, further glycosylation led to an increase in mass to 120 kDa (Milgram *et al.*, 1994b); no significant differences in the early stages of the biosynthesis of PAM-1 and PAM-1/K919R were observed. Cleavage to generate 45-kDa PHM was first apparent after 1 h of chase, with more 45-kDa PHM appearing during the second hour of chase (Figure 2B). The only difference apparent in

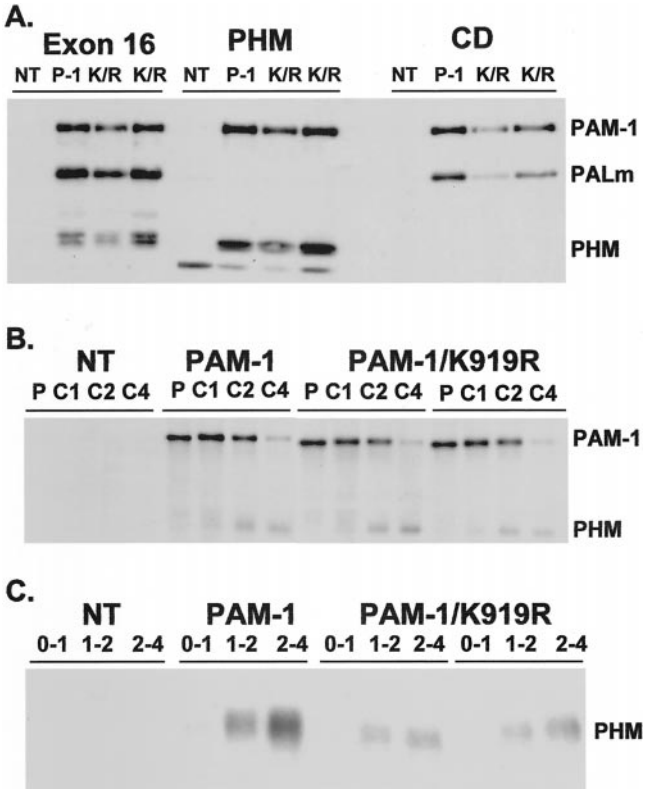

Figure 2. PAM-1/K919R is Active, cleaved, and retained within the cell. (A) Western blot analysis. Aliquots of nontransfected (NT) AtT-20 cells and AtT-20 cells expressing PAM-1 (P-1) or PAM-1/K919R (K/R; 2 independent clones) yielding equal amounts of PAL activity were fractionated on 10% SDS polyacrylamide gels. PAM proteins transferred to polyvinylidene difluoride membranes were visualized with antisera to exon 16, PHM (JH1761), or PAM-CD (JH571). (B) Metabolic labeling. Quadruplicate wells of each cell type were labeled with [^{35}S]Met for 15 min and either extracted immediately (P) or chased with nonradioactive medium for 1 (C1), 2 (C2), or 4 (C4) h before extraction and immunoprecipitation with antiserum to PHM. (C) Basal secretion. During the 4-h chase, medium was collected sequentially from 0–1, 1–2, and 2–4 h; PHM proteins were immunoprecipitated. Incorporation of [^{35}S]Met into trichloroacetic acid-precipitable material was similar for the different cell lines.

the metabolism of the two PAM proteins was decreased basal secretion of newly synthesized 45-kDa PHM by PAM-1/K919R cells (Figure 2C); this observation suggests differences in secretory granule function.

Misfolded proteins are generally retained in the endoplasmic reticulum and membrane proteins lacking trafficking information often accumulate on the plasma membrane. Based on simultaneous staining for PHM and CD, much of the PAM-1/K919R is localized to the perinuclear region (Figure 3A, thick arrows), with some staining in cellular processes (Figure 3A, asterisks). Visualized with the same antisera, PAM-1 is localized to a much more compact structure (Figure 3A). Simultaneous staining for PAM and γ-adaptin, a component of the AP1 adaptor complex (Schmid and Damke, 1995; Robinson, 1997; Schmid, 1997) identifies the PAM-containing region of the cell as the TGN (Figure 3B). In PAM-1/K919R cells, variably sized punctate structures scattered throughout the cytoplasm (Figure 3A, thin arrows) and at the tips of processes (Figure 3A, asterisks) were also visualized by PAM antisera. These punctate structures were distinct from mannose 6-phosphate receptor containing structures (Figure 3B) or lysosomes and were not observed in PAM-1 cells (Figure 3A).

Another key feature of PAM trafficking is endocytosis from the plasma membrane (Milgram *et al.*, 1993; Steveson *et al.*, 1999). At steady state, ~5% of the PAM protein resides on the cell surface, and internalization of antibody directed to the ectodomain of PAM is easily observed (Tausk *et al.*, 1992; Milgram *et al.*, 1996; Steveson *et al.*, 1999). AtT-20 cells expressing PAM-1/K919R or PAM-1 were incubated with antibody to the PAM luminal domain and chased in serum-free medium before visualization of the internalized antibody (Figure 3C). After a 5-min chase, internalized PAM/PAM antibody complexes were prevalent in early endosomes distributed throughout the cell. A longer chase time allowed PAM/PAM antibody complexes to collect in the TGN region. No dramatic differences in PAM/PAM antibody internalization were observed between cells expressing PAM-1/K919R and PAM-1.

Lys^{919} Is Essential for the Effect of PAM on Cytoskeletal Organization

Two of the PAM-CD interactors identified with the yeast two-hybrid screen could link PAM to the cytoskeleton. P-CIP2 interacts with stathmin, which can control the state of polymerization of microtubules (Horwitz *et al.*, 1997; Maucuer *et al.*, 1997). Kalirin interacts with Rac1, promoting exchange of GDP for GTP (Alam *et al.*, 1997), and activated Rac1 affects the actin cytoskeleton (Hall, 1998). Consistent with this, we showed previously that expression of membrane PAM causes rearrangement of the actin cytoskeleton (Ciccotosto *et al.*, 1999), as does expression of Kalirin (Mains *et al.*, 1999; Penzes *et al.*, 2000).

Filamentous actin was visualized in nontransfected, PAM-1/K919R, and PAM-1-transfected AtT-20 cells using FITC-phalloidin (Figure 4). In nontransfected AtT-20 cells, filamentous actin was distributed in brightly stained patches throughout much of the cytoplasm, with some staining at the margins of cells (Figure 4, #). Filopodia were prominent on a significant number of the nontransfected cells (Figure 4, asterisks). As described earlier, expression of PAM-1 changed the organization of filamentous actin in AtT-20 cells; overall staining intensity was lower, with diffuse staining throughout the cell and patches of filamentous actin often collected in the TGN region, where PAM-1 is localized; filopodia were rarely observed, and cortical actin was not prominent at the margins of the cells. A distinctly different distribution of filamentous actin was observed in AtT-20 cells expressing PAM-1/K919R; intense staining for filamentous actin often outlined the cell margins (Figure 4, #). In a subset of large, polygonal flat cells, lengthy stretches of subplasma membrane filamentous actin were punctuated by bright foci of FITC-phalloidin staining at the vertices. Although patches of filamentous actin were scattered widely throughout the cell, the most intense staining was generally at the cell surface, with no concentration of filamentous actin observed in the perinuclear region. Filopodia were com-

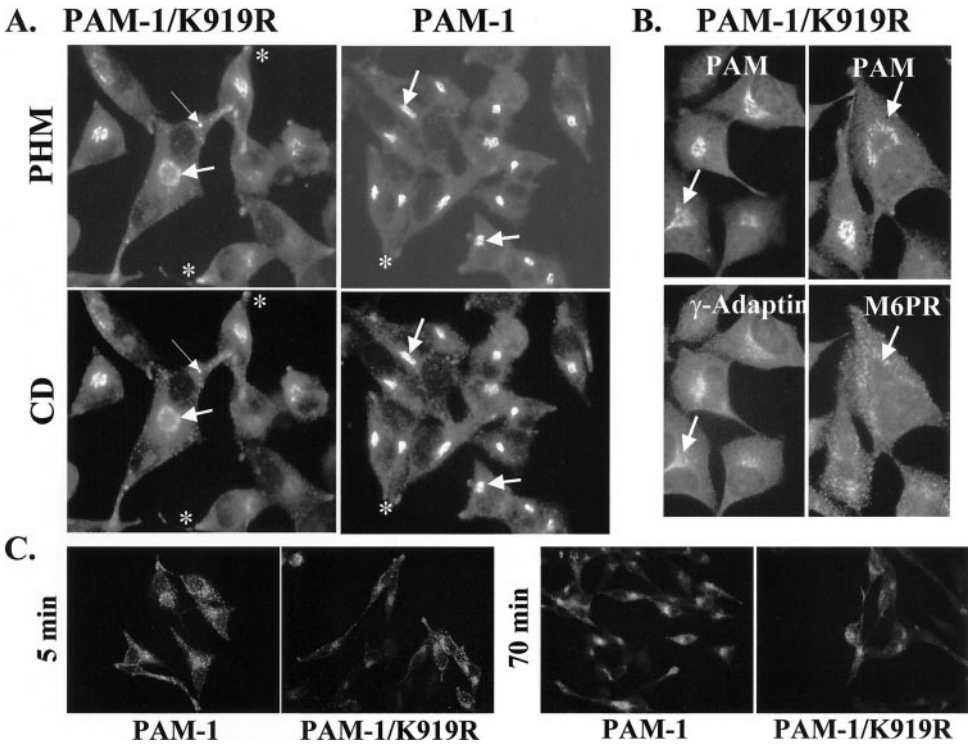

Figure 3. PAM-1/K919R cells: localization and internalization of PAM antibody. (A) AtT-20 cells expressing PAM-1/K919R or PAM-1 were visualized simultaneously with rabbit polyclonal antiserum to PHM (JH1761) and mouse monoclonal antibody to PAM-CD. Bold arrows mark the TGN region and thin arrows indicate sites of vesicular staining and asterisks mark tips of processes. (B) AtT-20 cells expressing PAM-1/K919R were visualized simultaneously with antisera to exon 16 and γ-adaptin or mannose 6-phosphate receptor (M6PR). Arrows mark identical sites in the TGN region. The images shown are representative of the staining patterns observed in multiple independently derived cell lines. (C) AtT-20 cells expressing PAM-1/K919R or PAM-1 were incubated in antibody to exon 16 for 10 min. Antibody was removed and cells were rinsed and chased for 5, 30, or 70 min before fixation and incubation with FITC-tagged goat anti-rabbit immunoglobulin. Identical results were obtained with two additional, independent PAM-1/K919R cell lines.

monly observed extending from the surface of PAM-1/K919R cells (Figure 4, asterisks).

Photographs of nontransfected cells, two clones of PAM-1/K919R cells, and PAM-1 cells were scored for total number of cells, cells with filopodia, and cells with prominent cortical actin bundles (Figure 4). The percentage of AtT-20 cells with filopodia (Figure 4, asterisk; $P < 0.03$) or cortical actin bundles (Figure 4, #; $P < 0.02$) was significantly higher in cells expressing PAM-1/K919R than in cells expressing PAM-1. Lys^{919} thus plays an essential role in the interaction of PAM with the actin cytoskeleton.

Lys^{919} Is Essential for the Effect of PAM on Regulated Secretion

Along with its effect on cytoskeletal organization, membrane PAM reduces the ability of secretagogues to stimulate secretion by AtT-20 cells (Ciccotosto *et al.*, 1999). We evaluated the role of Lys^{919} in this response by examining the basal and stimulated secretion of PHM, ACTH, and PC1 in AtT-20 cells expressing PAM-1/K919R (Figure 5). After two basal collection periods, cells were stimulated by incubation with medium containing 1 mM $BaCl_2$ (Ratovitski *et al.*, 1999). $BaCl_2$ was used as an effective, reproducible secretagogue capable of stimulating secretion from mature granules (Mains and Eipper, 1981).

Nontransfected cells secreted detectable levels of PHM activity under basal conditions, and addition of $BaCl_2$ resulted in a fourfold (2.5- to 7-fold range; $P < 0.001$ compared with basal) increase in PHM secretion (Figure 5A). As observed previously, PAM-1-expressing AtT-20 cells secreted high levels of PHM activity under basal conditions, and treatment with $BaCl_2$ failed to stimulate secretion as effectively as in wild-type cells (1.23 ± 0.13-fold; $P = 0.26$ with respect to basal secretion). Basal secretion of PHM activity from PAM-1/K919R cells was not as high as from PAM-1 cells, despite the similar specific activity of cell extracts. Unlike the PAM-1 cells, the PAM-1/K919R cells responded robustly to $BaCl_2$; PHM secretion was increased 4.5-fold (range 3- to 7-fold; $P < 0.002$) over basal levels. Aliquots of medium were also subjected to Western blot analysis (Figure 5B). Basal secretion of 45-kDa PHM from PAM-1/K919R cells was lower than from PAM-1 cells and was stimulated upon inclusion of $BaCl_2$. In contrast, little stimulation of secretion of 45-kDa PHM was observed for PAM-1 cells. The differences observed in the basal and stimulated secretion of PHM suggest that expression of PAM affects formation of regulated secretory granules.

We next examined the basal and stimulated secretion of two additional secretory granule products, ACTH (Figure 5C) and PC1. AtT-20 cells produce POMC and cleave it to generate ACTH, which is stored in secretory granules (Ratovitski *et al.*, 1999). PC1 is responsible for the initial cleavage of POMC as well as the subsequent cleavages that produce ACTH (Mains *et al.*, 1991). Secretion of ACTH from AtT-20 cells expressing PAM-1/K919R was as responsive to stimulation by $BaCl_2$ (4.5-fold; range 3- to 6-fold) as secretion of ACTH from nontransfected cells (6-fold; range 4- to 7-fold). In contrast, as observed previously, secretion of ACTH by AtT-20 cells expressing PAM-1 was unaltered by $BaCl_2$ (1.2 ± 0.2-fold; $P > 0.25$). We used metabolic labeling to establish that the rate of POMC biosynthesis in the different cell types was indistinguishable (data not shown). Addition of secretagogue also increases the secretion of ma-

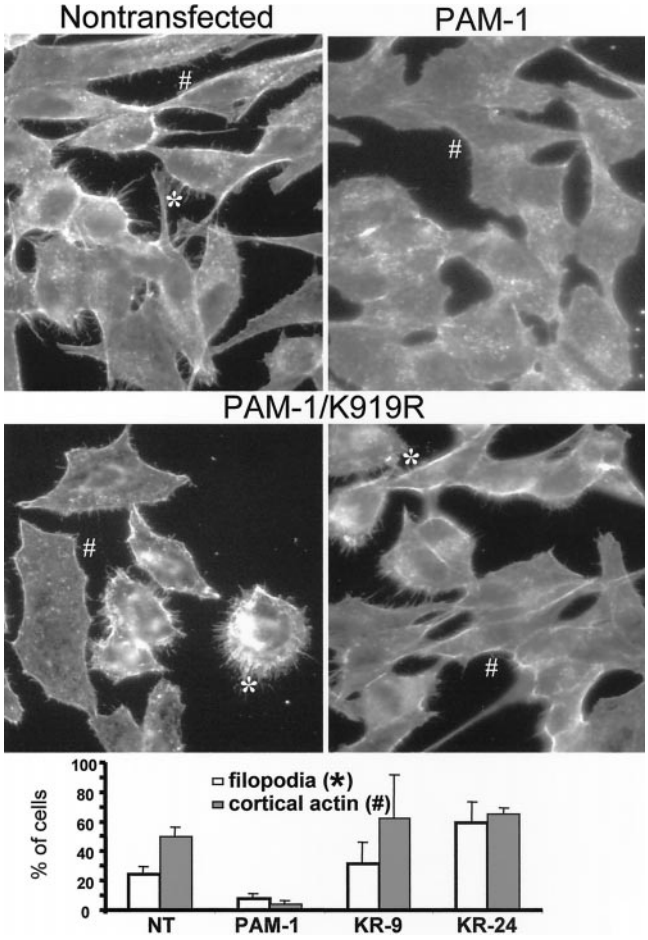

Figure 4. PAM-1/K919R and PAM-1 have different effects on cytoskeletal organization in AtT-20 cells. The filamentous actin in nontransfected, PAM-1, and PAM-1/K919R-expressing AtT-20 cells was visualized with FITC-phalloidin. Four micrographs of each cell type were scored for total cell number, cells with filopodia (*), and cells with cortical actin (#); 200 cells were counted for each cell type by an observer unaware of the identity of the cells, and data are the average for the four micrographs of a given cell type ± SD.

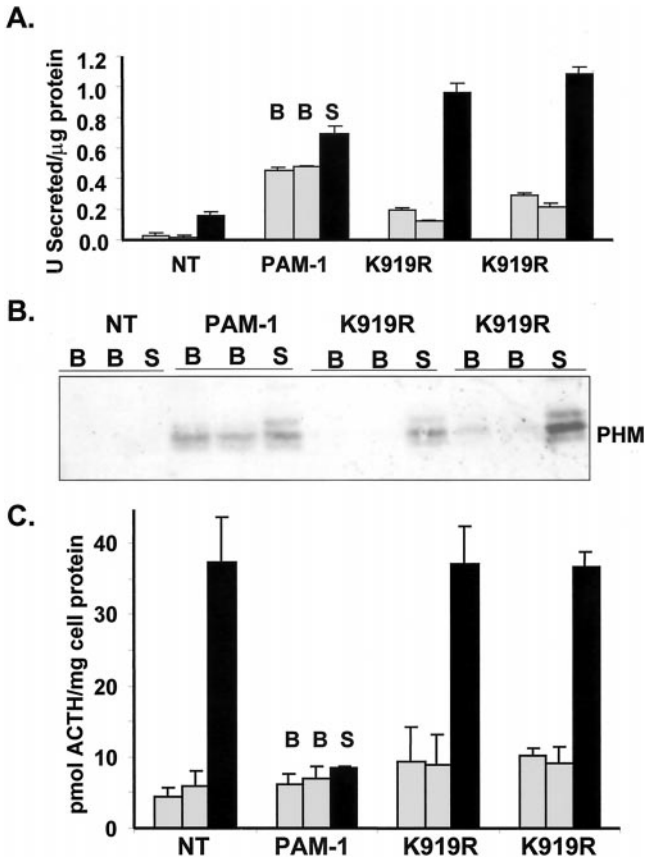

Figure 5. Secretion from PAM-1/K919R cells is responsive to secretagogue. (A) Triplicate wells of nontransfected (NT), PAM-1, and two PAM-1/K919R (9C and 24C) AtT-20 cell lines were equilibrated with complete serum-free medium; medium was collected for two 30-min periods under basal conditions (B) followed by one 30-min period in the presence of 1 mM $BaCl_2$ (S). PHM activity (1 unit = 1 pmol/h) secreted in each 30-min period is normalized to total cell protein. Error bars represent SD for duplicate determinations of triplicate samples. (B) Medium collected during one secretion experiment was fractionated by SDS-PAGE, and secreted PAM proteins were visualized using antiserum to exon 16. The entire experiment was replicated twice with similar results. (C) A secretion experiment was carried out on quadruplicate wells of cells. Secreted ACTH was quantified using a radioimmunoassay. SDs are shown by error bars. The entire experiment was replicated with similar results. The same cell lines were incubated in medium containing [^{35}S]Met for 15 min, extracted in 5 N acetic acid, and immunoprecipitated using antiserum to ACTH; POMC synthesis was indistinguishable.

ture PC1 by nontransfected and PAM-1/K919R cells but not by PAM-1 cells.

Although the mechanism through which expression of PAM-1 inhibits stimulated secretion by AtT-20 cells has not been elucidated, the fact that PAM-1/K919R can be expressed at the same level without the same effect establishes the specificity of the response and supports a role for interactors specific to the Lys^{919} site in the process. The fact that PAM-1 affects both basal and stimulated secretion of multiple secretory granule proteins suggests alterations in regulated secretory granule formation and/or storage.

Expression of PAM-1, but Not PAM-1/K919R, Causes Accumulation of PAM and ACTH in Tubular Structures

Along with its inhibitory effect on regulated secretion, expression of membrane PAM causes an accumulation of ACTH in the TGN region of AtT-20 cells (Ciccotosto *et al.*, 1999). We compared the localization of ACTH in nontransfected, PAM-1/K919R, and PAM-1-expressing AtT-20 cells using immunofluorescence microscopy (Figure 6); PAM proteins were simultaneously visualized using antisera to the cytosolic domain of PAM. In nontransfected AtT-20 cells, ACTH is concentrated in mature secretory granules and vesicular structures collected at the tips of cellular processes (Figure 6, asterisks); endogenous PAM levels are too low to visualize (Figure 6A; Schnabel *et al.*, 1989; Tooze *et al.*, 1989). As observed previously, in AtT-20 PAM-1 cells, ACTH is

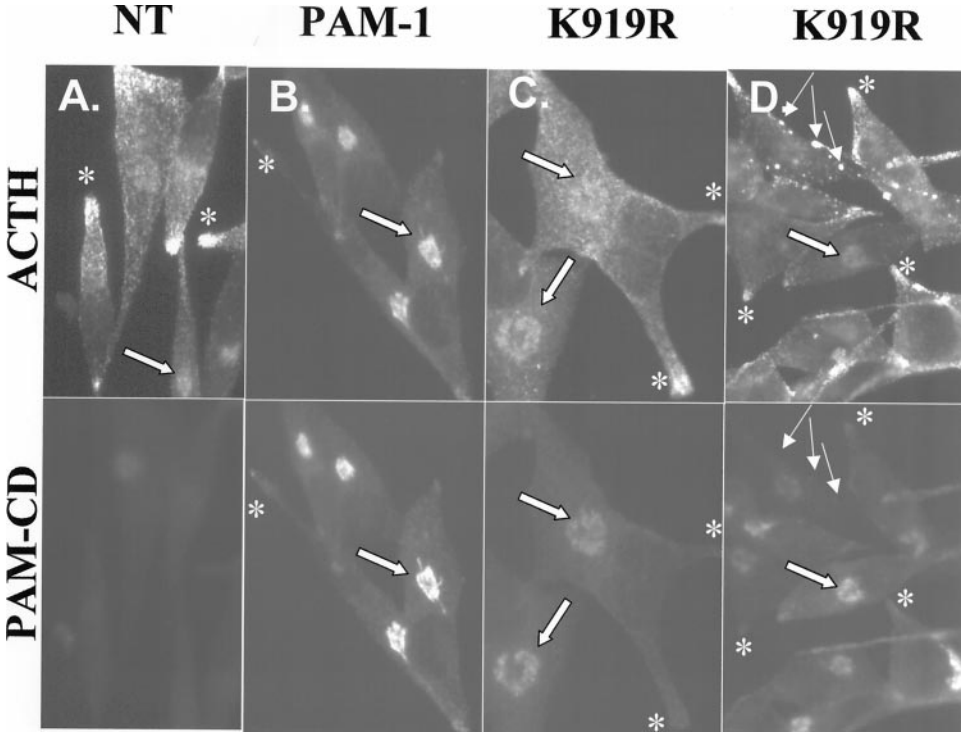

Figure 6. ACTH localization in PAM-1/K919R Cells. Nontransfected (A), PAM-1 (B), and PAM-1/K919R (C and D) AtT-20 cells were visualized simultaneously with rabbit polyclonal ACTH antiserum (top; JH93) and mouse monoclonal antibody to the CD of PAM (bottom). Asterisks indicate the tips of processes; thin arrows indicate large vesicular structures; thick arrows indicate the TGN region.

localized to the TGN region instead of at the tips of processes and is largely coincident with staining for PAM (Figure 6B, thick arrows). In cells expressing PAM-1/K919R, ACTH staining is not concentrated in the TGN region; ACTH-containing vesicular structures are distributed throughout the cytosol (Figure 6B, narrow arrows), with ACTH staining observed at the tips of processes (Figure 6, C and D). At the light microscopic level, the ACTH-containing vesicular structures in AtT-20 PAM-1/K919R cells contain PHM and are distinct from lysosomes, which contain lysosome-associated membrane protein 1.

The more diffuse staining pattern of PAM in PAM-1/K919R cells (Figure 6, C and D) compared with PAM-1 cells (Figure 6B) suggested there might be important ultrastructural differences in the localization of membrane PAM in the two cell types. Immunoelectron microscopy was used to compare the localization of PAM in AtT-20 cells expressing PAM-1/K919R and PAM-1 (Figure 7). PAM-1 cells (Figure 7, A and B) clearly show more dense staining for PAM in tubular structures in the TGN than do PAM-1/K919R cells (Figure 7D). In PAM-1/K919R cells, more of the PAM staining is in rounded rather than tubular structures (Figure 7D). These observations were quantified by counting the number of gold particles over the *trans*-Golgi area: 104 ± 16 (SEM) per *trans*-Golgi area in PAM-1 cells (n = 20) versus 44 ± 5 per *trans*-Golgi area in PAM-1/K919R cells (n = 17). Of these gold particles, 5% were associated with rounded structures in PAM-1 cells, whereas 12% were associated with rounded structures in PAM-1/K919R cells. This is reflected in the somewhat higher frequency of gold particles in mature secretory granules from PAM-1/K919R cells (Figure 7E) compared with PAM-1 cells (Figure 7C). When a tubular structure in an AtT-20 PAM-1 cell is stained for PAM, gold particles are generally arrayed along the entire extent of the tubule, which is often filled with electron-dense material (Figure 7B). Accumulation of secretory proteins in the TGN was also notable as aggregations of electron-dense material in conventional electron microscopic sections; these condensations were seen in 31 of 83 *trans*-Golgi areas in PAM-1 cells (Figure 7, F–H) but in only 4 of 75 *trans*-Golgi areas in PAM-1/K919R cells (Figure 7I). These structures were not seen in nontransfected AtT-20 cells.

The light microscopic indication of more diffuse PAM immunostaining in the TGN region of PAM-1/K919R cells could reflect a more extensive tubular organization of the TGN in these cells. The sparser PAM immunostaining seen by electron microscopy would simply reflect this broader distribution. To investigate this possibility, the number of transections of tubular and vesicular structures in a 1-μm wide area along the *trans* side of the Golgi cisterns was quantified. No significant difference between PAM-1 and PAM-1/K919R cells was observed: 55 ± 6 elements/μm^2 in PAM-1 cells; 67 ± 5 elements/μm^2 in PAM-1/K919R cells (SEM, P = 0.14; n = 14 and 15 cells, respectively, systematically sampled from three different experiments). Thus, the decreased PAM concentration in PAM-1/K919R cells is not due to a difference in TGN architecture.

Cryosections were visualized simultaneously with antisera to PAM (10-nm gold) and to ACTH (15-nm gold). The PAM-containing electron-dense tubular structures observed in AtT-20 PAM-1 cells also contain ACTH (Figure 8, A and C). The PAM-containing vesicular structures observed in PAM-1/K919R cells are visualized by antisera to ACTH (Figure 8B). Given the localization of these ACTH-containing structures, we consider them to be immature secretory granules. Mature secretory granules are characterized by

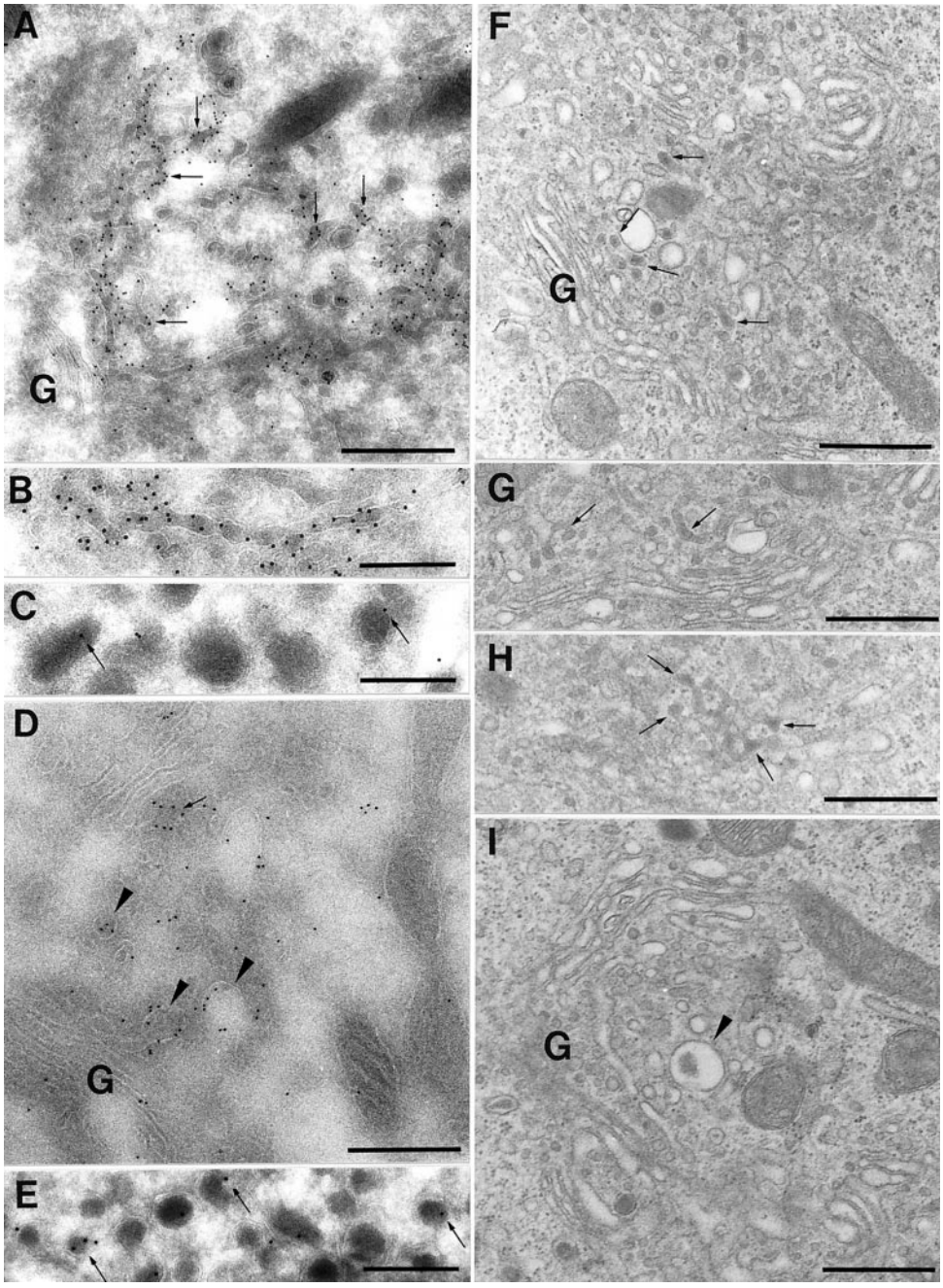

Figure 7. Ultrastructural analysis of AtT-20 cells expressing PAM. (A–E) Immunoelectron microscopy. PAM staining in tubular or vesicular structures (arrows) and rounded structures (arrowheads) at the *trans* side of Golgi cisterns (G) in PAM-1 (A and B) and PAM-1/K919R (D) cells. PAM staining in mature secretory granules (arrows) in PAM-1 cells (C) and PAM-1/K919R cells (E). Scale bar, 0.5 μm (A, D) or 0.25 μm (B, C, E). (F–I) Electron microscopy. Golgi area of PAM-1 cells (F–H) and a PAM-1/K919R cell (I) showing electron-dense condensations in the TGN (arrows) only in PAM-1 cells. A typical immature secretory granule is shown at the arrowhead in I. Scale bar, 0.5 μm.

their uniform content of electron-dense material and their localization near the plasma membrane. In both cell types, the mature secretory granules contain PAM and ACTH; the ratio of ACTH staining to PAM staining is increased substantially over the ratio observed in tubular or vesicular structures observed in the perinuclear, TGN region of the cell.

Interactions of PAM with P-CIP2 Are Critical

PAM-1/K919R loses the ability to interact with both Kalirin and P-CIP2 and perhaps with other as yet unidentified proteins (Table 1). In contrast, mutation of Leu^{926} to Gln or of Phe^{929} or Phe^{930} to Ser eliminated the ability of PAM-CD to interact with P-CIP2 in the liquid-phase β-galactosidase assay while leaving the Kalirin interaction intact (Table 1). Therefore we sought to use these more selective mutants to distinguish roles for P-CIP2 and Kalirin. If an interaction with P-CIP2 were essential to the ability of PAM to affect the regulated secretory pathway, AtT-20 cells expressing a PAM protein that could interact with Kalirin, but not with P-CIP2, would mimic the behavior of PAM-1/K919R.

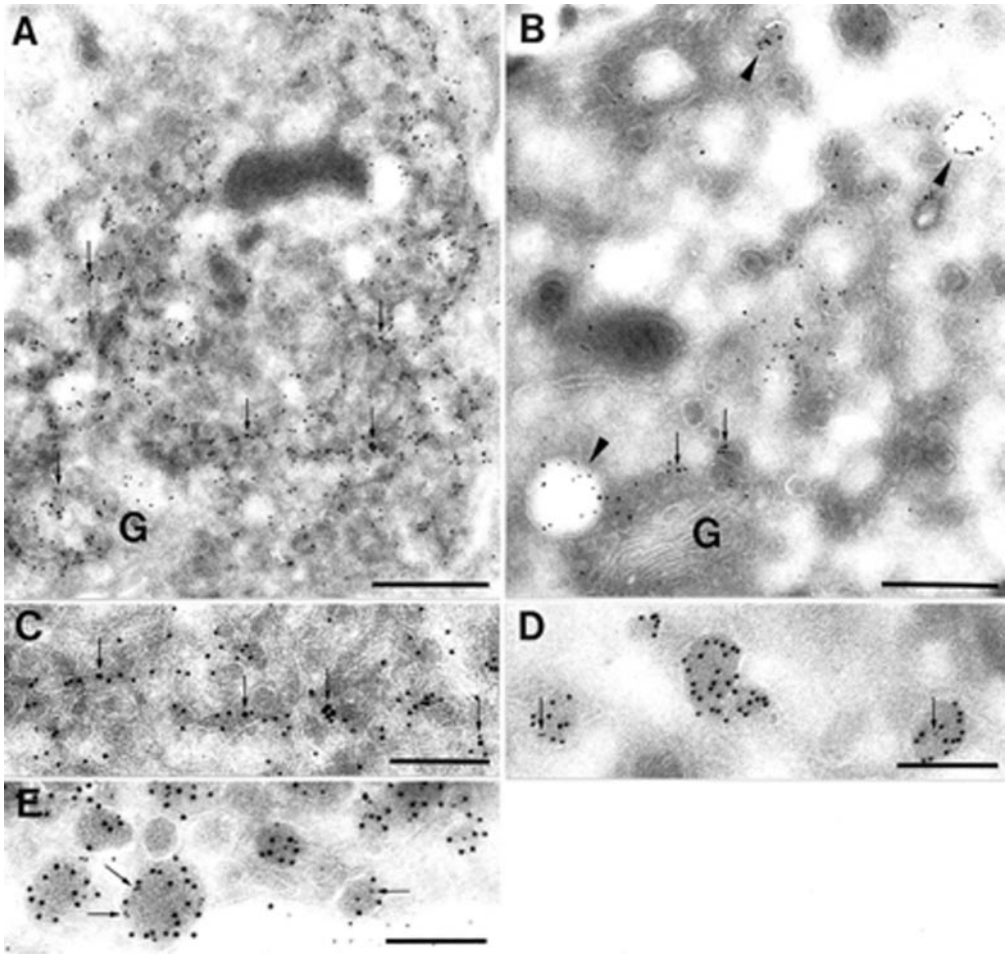

Figure 8. Immunoelectron microscopy. Simultaneous PAM (10-nm gold) and ACTH (15-nm gold) staining in tubular structures in the TGN (arrows) and rounded structures (arrowheads) in PAM-1 cells (A and C) and PAM-1/K919R cells (B). Scale bars, 0.5 μm (A and B); 0.25 μm (C).

We designed two PAM proteins to test this hypothesis: in one, Leu^{926} was mutated to Gln (PAM-1/L926Q); in the other, Phe^{929} and Phe^{930} were mutated to Ala (PAM-1/FF/AA). Nontransfected cells and AtT-20 cells expressing PAM-1/L926Q or PAM-1/FF/AA were visualized simultaneously with antisera to PAM (red) and ACTH (green) (Figure 9). As documented previously, ACTH staining in nontransfected AtT-20 cells is vesicular, with vesicles accumulating at the tips of processes (Figure 9, NT). AtT-20 cells stably expressing PAM-1/L926Q exhibit PAM staining in the TGN area with ACTH staining in vesicular structures that accumulate at the tips of cellular process and are not concentrated in the TGN area (Figure 9). AtT-20 cells stably expressing PAM-1/FF/AA also exhibit ACTH staining much like that observed in nontransfected cells. In contrast, ACTH staining in PAM-1 cells is coincident with PAM staining in the TGN area (Figure 6). Thus, the ability of PAM to disrupt normal trafficking in the regulated secretory pathway depends on its ability to interact with P-CIP2 or with an unidentified interactor with similar binding specificity. The interaction of PAM with Kalirin is not essential for this response.

P-CIP2 phosphorylates Ser^{949} in the cytosolic domain of PAM (Caldwell *et al.*, 1999), a site distinct from those identified in the yeast two-hybrid screen (Table 1). To ask whether P-CIP2-mediated phosphorylation of PAM-CD might play an essential role in this process, we generated stably transfected AtT-20 cell lines expressing PAM-1 in which both Ser^{949} and Thr^{946} were mutated to either Ala or to Asp (PAM-1/TS/AA and PAM-1/TS/DD). Mutation to Ala would prevent phosphorylation , whereas mutation to Asp might mimic the presence of phosphorylated Ser and Thr (Steveson *et al.*, 1999). We chose to mutate Thr^{946} along with Ser^{949} because phosphorylation of Ser^{949} could render Thr^{946} a potential substrate for kinases with casein kinase II-like specificity; such kinases play important roles in the trafficking of many membrane proteins (Jones *et al.*, 1995; Wan *et al.*, 1998).

The regulated secretory pathway was disrupted in AtT-20 cells expressing PAM-1/TS/AA. Secretagogue failed to stimulate release of immunoreactive ACTH (Figure 10A), and ACTH staining was not concentrated at the tips of cellular processes (Figure 10B). In contrast, in cells expressing PAM-1/TS/DD, the regulated secretory pathway more closely resembled that in wild-type AtT-20 cells. Secretory granules were dispersed throughout the cell, with some accumulation at the tips of processes (Figure 10B), and addition of secretagogue produced a 5-fold stimulation in the secretion of immunoreactive ACTH (Figure 10A).

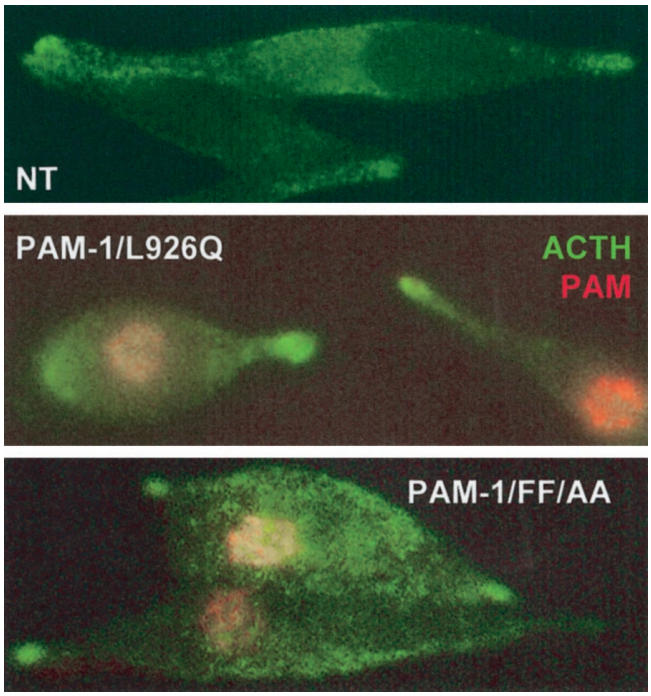

Figure 9. Mutations that eliminate P-CIP2 binding mimic the K919R mutation. Stably transfected AtT-20 cell lines expressing PAM-1/Leu926Gln (L926Q) or PAM-1/PhePhe929,930AlaAla (FF/AA) were fixed and visualized simultaneously with a monoclonal antiserum to the cytosolic domain of PAM (6E6) and a polyclonal antiserum to ACTH (JH93). Green arrows mark areas in which ACTH-containing vesicles are concentrated; red asterisks mark the TGN area. At least two cell lines for each mutant were examined with similar results.

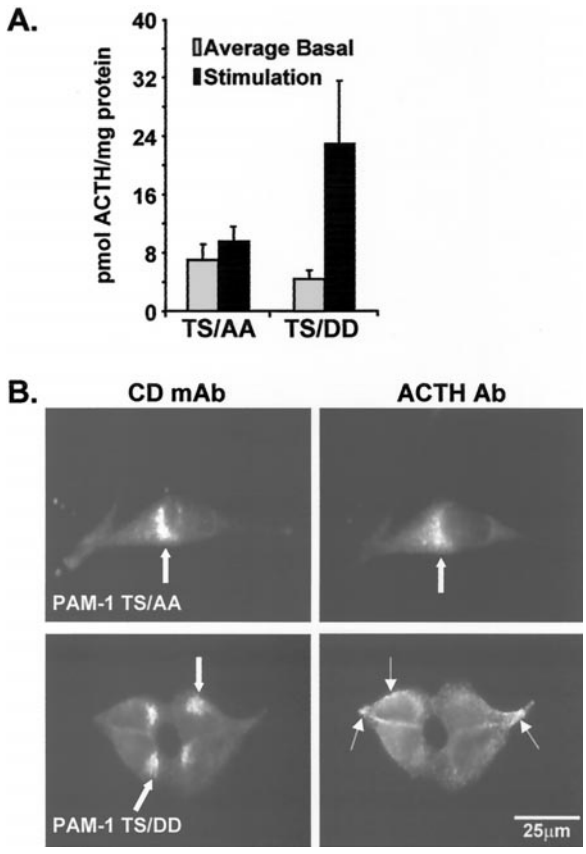

Figure 10. Mutation of P-CIP2 phosphorylation site in PAM-CD affects regulated secretion. (A) AtT-20 PAM-1 TS/AA and PAM-1 TS/DD cells were subjected to a secretion study as in Figure 5. Secreted ACTH was quantified by radioimmunoassay. The levels of ACTH from the two basal secretion samples were averaged separately for each cell line. Experiments were performed in triplicate. (B) AtT-20 cells expressing PAM-1/TS/AA and PAM-1/TS/DD were fixed with 4% paraformaldehyde, permeabilized, and doubly immunostained with a monoclonal antibody to the CD-PAM and an ACTH polyclonal antibody. Wide arrows show immunostaining in the perinuclear/TGN region, and narrow arrows show staining in the cellular processes and tips.

DISCUSSION

P-CIP2 and Kalirin Recognize Overlapping but Distinct Motifs in the CD of PAM

By using random mutagenesis, we identified the features of PAM-CD required for its interaction with P-CIP2 and Kalirin. Both interactions are eliminated by mutation of Lys^{919} to Arg (K919R) or Met (data not shown); because truncation of PAM at Tyr^{936} eliminates its normal trafficking in AtT-20 cells as effectively as truncation immediately after the transmembrane domain (at Gly^{899}), the membrane proximal region of PAM had not been identified as important. The failure of Arg to substitute for Lys^{919} indicates that the simple presence of a large, positively charged amino acid at this position is not adequate. The fact that the ϵ-NH_2-group of Lys is the site of 40 posttranslational modifications may explain its essential role (Wold, 1981; Hand *et al.*, 1994; Park *et al.*, 1998; Thornalley, 1998). Although Lys residues of some membrane proteins are subject to ubiquitination (Hicke and Riezman, 1996; Roth and Davis, 1996), we found no evidence for ubiquitination of PAM using antisera to ubiquitin to visualize immunoprecipitated protein (data not shown). Consistent with the importance of this site, the -Arg-Gly-Lys^{919}-Gly-Ser-Gly-Gly- sequence is conserved from *Xenopus* to human.

In addition to Lys^{919}, the interactions of P-CIP2 and Kalirin with the CD-PAM require additional residues located further from the transmembrane domain. Our previous studies indicated that cytosolic residues 928–945 were important in facilitating access of PAM to secretory granules (Milgram *et al.*, 1996), and identification of P-CIP2 and Kalirin relied on this fact. Our mutagenesis studies indicate that P-CIP2 requires Phe^{929} and Phe^{930} and Kalirin requires Tyr^{936}, a residue known to play a critical role in the internalization of PAM from the surface of AtT-20 cells (Milgram *et al.*, 1996). In contrast, mutation of Ser^{937} to Gly failed to affect the interaction of PAM with Kalirin or P-CIP2, suggesting that these proteins do not play a role in steps sensitive to phosphorylation of this residue (Yun *et al.*, 1995; Steveson *et al.*, 1999). Importantly, mutation of Ser^{949}, the site phosphorylated by P-CIP2, to Ala or Asp did not eliminate the ability of P-CIP2 to interact with PAM (Caldwell *et*

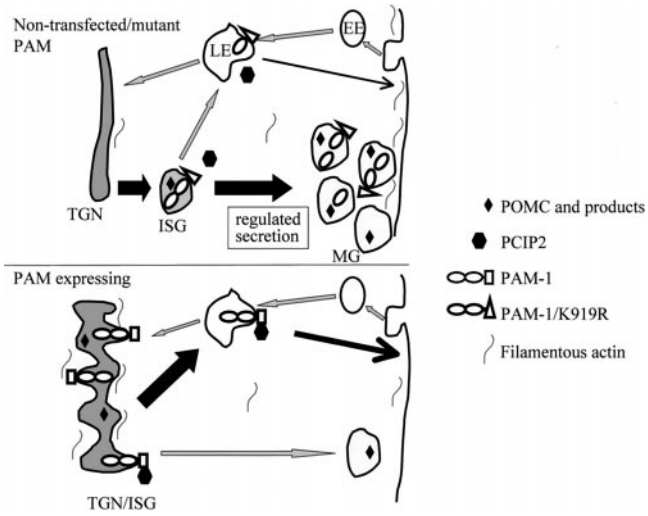

Figure 11. Model. Trafficking of PAM from the TGN to immature and mature secretory granules and through the endocytic pathway is compared in nontransfected AtT-20 cells (top), AtT-20 cells expressing PAM-1/K919R (top), and AtT-20 cells expressing PAM-1 (bottom). See text for discussion of model. LE, late endosome; EE, early endosome; ISG, immature secretory granule; MG, mature granule.

al., 1999). Thus, the P-CIP2-binding and phosphorylation sites in CD-PAM are distinct. Although the Tyr motif and phosphorylation sites in PAM resemble motifs important in the trafficking of furin (Dittie *et al.*, 1999) and carboxypeptidase D (Varlamov *et al.*, 1999), membrane proteins that also enter immature secretory granules, Lys^{919}, in PAM are unique.

Lys^{919} Plays a Key Role in the Effect of PAM on Regulated Secretion

Because mutation of Lys^{919} to Arg is a conservative change, and yet completely blocks the ability of CD-PAM to interact with either Kalirin or P-CIP2, we used AtT-20 lines expressing similar levels of each protein to evaluate the importance of interactions mediated by Lys^{919}. PAM-1/K919R and PAM-1 yield fully active enzymes, with similar endoproteolytic cleavage products; both proteins begin to yield 45-kDa PHM at similar chase times, indicating that they enter a cleavage-competent compartment with similar kinetics (Milgram and Mains, 1994; Figure 11). Despite its inability to interact with endogenous P-CIP2 and any endogenous Kalirin-like proteins, PAM-1/K919R does not accumulate on the cell surface and is internalized efficiently. In contrast, PAM proteins truncated immediately after the transmembrane domain or at Tyr^{936} adopt a plasma membrane localization and fail to undergo internalization (Milgram *et al.*, 1996).

Despite these similarities, AtT-20 cells expressing PAM-1 and PAM-1/K919R exhibit distinct differences (Figure 11). Expression of PAM-1 eliminates the filopodia observed in nontransfected cells, perhaps reflecting interactions with an endogenous Kalirin-like protein; in contrast, filopodia are prevalent in PAM-1/K919R cells. Based on immunofluorescence, both PAM-1 and PAM-1/K919R are localized to the TGN area (Figure 3). However, immunoelectron microscopy reveals distinct differences in the localization of both PAM and ACTH in the two cell types. In PAM-1/K919R cells, PAM- and ACTH-containing immature secretory granules can be identified near the Golgi. In contrast, in PAM-1 cells, immature secretory granules are rare and PAM and ACTH are localized to tubular structures at the *trans* side of the Golgi (Figures 7 and 8; Milgram *et al.*, 1997). Because expression levels are similar, this observation suggests that PAM-1 leaves these tubular structures more slowly than PAM-1/K919R. Using an AtT-20 line in which expression of PAM-1 is inducible, we previously demonstrated that increasing PAM-1 expression causes a decreasing ability of AtT-20 cells to store PHM, ACTH, and PC1 in granules and to secrete these products in response to secretagogue (Ciccotosto *et al.*, 1999; Mains *et al.*, 1999). Mutation of Lys^{919} to Arg eliminates the ability of PAM-1 to exert this effect on the regulated secretory pathway. Stimulated secretion of PHM, ACTH, and PC1 is comparable in cells expressing PAM-1/K919R and in nontransfected AtT-20 cells (Figure 5).

Signaling through P-CIP2 Allows PAM to Affect Trafficking in the Regulated Pathway

Our goal in designing PAM proteins unable to interact with P-CIP2 or Kalirin was to test the hypothesis that these interactors or other proteins interacting at the same sites were essential to the normal function of PAM. Our analysis of the phenotype of the PAM-1 mutants clearly identifies a role for the cytosolic domain in secretory granule formation, in addition to its previously identified role in PAM trafficking (Milgram *et al.*, 1996; Steveson *et al.*, 1999). The formation of secretory granules is thought to be a signal mediated process, with roles proposed for small GTP-binding proteins, heterotrimeric G proteins, protein phosphorylation and dephosphorylation, and phospholipase D (Austin and Shields, 1997; Urbe *et al.*, 1997; Ktistakis, 1998; Tooze, 1998). As granules mature, they acquire responsiveness to secretagogue (Mains and Eipper, 1981; Arvan *et al.*, 1991), a process that involves removal of specific proteins (Kuliawat *et al.*, 1997; Eaton *et al.*, 2000).

As summarized diagrammatically in Figure 11, expression of PAM-1 diminishes the ability of AtT-20 cells to secrete PHM, ACTH, and PC1 in response to secretagogue (Ciccotosto *et al.*, 1999). Our immunoelectron microscopy demonstrates that overexpression of PAM-1 prevents the vesiculation/maturation of tubular structures on the *trans* side of the Golgi complex. There is an accumulation of electron-dense material, and entire tubules appear to contain PAM and ACTH (Figure 8). Formation of both immature and mature ACTH-containing granules is diminished. Secretion from these tubular structures is not responsive to secretagogue (Figure 5). These images are best fit by the cisternal maturation model of Golgi trafficking (Ladinsky *et al.*, 1995; Mironov *et al.*, 1997; Ladinsky *et al.*, 1999; Pelham, 2000). The localized presence of a larger than normal amount of polymerized actin may contribute to this effect (Figure 4). In contrast, expression of PAM-1/K919R does not cause accumulation of ACTH and PAM in the TGN. Secretion of ACTH, PHM, and PC1 is responsive to secretagogue. Polymerized actin is not accumulated in the TGN region of cells expressing PAM-1/K919R.

Expression of PAM proteins capable of interacting with Kalirin but not with P-CIP2 (L926Q; FF/AA) does not impair regulated secretion (Figure 9). Thus, the ability of PAM to interact with P-CIP2 or another protein with similar binding specificity is key to this phenotype. Analysis of AtT-20 cells expressing PAM proteins in which the P-CIP2 phosphorylation site has been eliminated (PAM-1/TS/AA) or mutated to mimic the end product (PAM-1/TS/DD) supports a key role for P-CIP2. Because expression of PAM-1/TS/AA eliminates the regulated secretion of ACTH, phosphorylation of PAM-CD by P-CIP2 is not essential for the inhibitory response. Regulated secretion from AtT-20 cells expressing PAM-1/TS/DD resembles regulated secretion from nontransfected cells. The need for P-CIP2 in progression from TGN to immature granules is bypassed by expressing a PAM protein that resembles the product of the actions of P-CIP2. Distinctly different roles can be ascribed to the binding of PAM to P-CIP2 and the phosphorylation of P-CIP2 by PAM.

It is not yet clear why overexpression of PAM in AtT-20 cells results in an accumulation of ACTH and PAM in the TGN and in impaired regulated secretion. Similar levels of PAM expression in primary pituitary cells do not impair regulated secretion (El Meskini *et al.*, 2000). Differences in the behavior of wild-type PAM-1 in AtT-20 cells and primary pituitary cells likely reflect deficits in the cell line (Matsuuchi and Kelly, 1991; Corradi *et al.*, 1996; Dannies, 1999). Imbalance of one partner in a multiprotein complex involving PAM and P-CIP2 may prevent progression. An excess of PAM over P-CIP2 may prevent P-CIP2 from interacting with other proteins or from phosphorylating PAM. Several features of the luminal domain of PAM suggest that it could play a role in cargo selection much like that proposed for membrane-spanning adaptor proteins in COPII-mediated trafficking from the endoplasmic reticulum (Kuehn and Herrmann, 1998): PHM is pH sensitive over the pH 7 to 5 range and PAM aggregates at low pH (Colomer *et al.*, 1996).

By eliminating the ability of PAM-1 to interact with P-CIP2 and perhaps with other proteins of similar binding specificity, we have identified a novel role for PAM in regulated secretion. Further studies will be required to determine the contributions of P-CIP2 and other PAM-CD interactors to each of the responses observed. A protein like Kalirin, with a spectrin-like repeat region and the ability to activate Rac1, a regulator of the actin cytoskeleton, could participate in processes that render the Golgi tubules susceptible or resistant to vesiculation (Lorra and Huttner, 1999) or could participate in the protein sorting functions of the membrane skeleton (Beck *et al.*, 1997; De Matteis and Morrow, 1998). P-CIP2, with its ability to phosphorylate sites that modify the ability of PAM to affect regulated secretion, appears to play a critical role in this process.

ACKNOWLEDGMENTS

We thank Tracey Hand for helping with the initial characterization of these cell lines, Lixian Jin and Marie Bell for making it possible to carry out these experiments, and Drs. Peter Penzes and Chenie Bell for helpful comments on the manuscript. N.B. thanks Anne Reijula, Reijo Karppinen, and Hannu Kamppinen for their help with this study and Professors Lars-Axel Lindberg and Antti Sukura for their support. This work was supported by National Institutes of Health grant DK-32948 (to R.E.M. and B.A.E.) and the K Albin Johansson Foundation and Finska Läkaresällskapet (N.B.).

REFERENCES

Alam, M.R., Caldwell, B.D., Johnson, R.C., Darlington, D.N., Mains, R.E., and Eipper, B.A. (1996). Novel proteins that interact with the COOH-terminal cytosolic routing determinants of an integral membrane peptide-processing enzyme. J. Biol. Chem. *271*, 28636–28640.

Alam, M.R., Johnson, R.C., Darlington, D.N., Hand, T.A., Mains, R.E., and Eipper, B.A. (1997). Kalirin, a cytosolic protein with spectrin-like, and GDP/GTP exchange factor-like domains that interacts with peptidylglycine α-amidating monooxygenase, an integral membrane peptide-processing enzyme. J. Biol. Chem. *272*, 12667–12675.

Arvan, P., Kuliawat, R., Prabakaran, D., Zavacki, A.M., Elahi, D., Wang, S., and Pilkey, D. (1991). Protein discharge from immature secretory granules displays both regulated and constitutive characteristics. J. Biol. Chem. *266*, 14171–14174.

Austin, C.D., and Shields, D. (1997). Formation of nascent secretory vesicles from the trans-Golgi network of endocrine cells is inhibited by tyrosine kinase and phosphatase inhibitors. J Cell. Biol. *135*, 1471–1483.

Beck, K.A., Buchanan, J.A., and Nelson, W.J. (1997). Golgi membrane skeleton: identification, localization and oligomerization of a 195 kDa ankyrin isoform associated with the Golgi complex. J Cell. Sci. *110*, 1239–1249.

Brown, M.S., and Goldstein, J.L. (1998). The SREBP pathway: regulation of cholesterol metabolism by proteolysis of a membrane-bound transcription factor. Cell *89*, 331–340.

Caldwell, B.D., Darlington, D.N., Penzes, P., Johnson, R.C., Eipper, B.A., and Mains, R.E. (1999). The novel kinase P-CIP2 interacts with the cytosolic routing determinants of the peptide processing enzyme peptidylglycine α-amidating monooxygenase. J. Biol. Chem. *274*, 34646–34656.

Chen, L., Johnson, R.C., and Milgram, S.L. (1998). P-CIP1, a novel protein that interacts with the cytosolic domain of peptidylglycine α-amidating monooxygenase, is associated with endosomes. J. Biol. Chem. *273*, 33524–33532.

Chevray, P.M., and Nathans, D. (1992). Protein interaction cloning in yeast: Identification of mammalian proteins that react with the leucine zipper of Jun. Proc. Natl. Acad. Sci. USA *89*, 5789–5893.

Ciccotosto, G.D., Schiller, M.R., Eipper, B.A., and Mains, R.E. (1999). Induction of integral membrane PAM expression in AtT-20 cells alters the storage and trafficking of POMC and PC1. J. Cell. Biol. *144*, 459–471.

Colomer, V., Kicska, G.A., and Rindler, M.J. (1996). Secretory granule content: proteins and the luminal domains of granule membrane proteins aggregate in vitro at mildly acidic pH. J. Biol. Chem. *271*, 48–55.

Corradi, N., Borgonovo, B., Clementi, E., Bassetti, M., Racchetti, G., Consalez, G.G., Huttner, W.B., Meldolesi, J., and Rosa, P. (1996). Overall lack of regulated secretion in a PC12 variant cell clone. J. Biol. Chem. *271*, 27116–27124.

Dannies, P.S. (1999). Protein hormone storage in secretory granules: mechanisms for concentration and sorting. Endocr. Rev. *20*, 3–21.

De Matteis, M.A., and Morrow, J.S. (1998). The role of ankyrin and spectrin in membrane transport and domain formation. Curr. Opin. Cell Biol. *10*, 542–549.

Dintzis, S.M., Velculescu, V.E., and Pfeffer, S.R. (1994). Receptor extracellular domains may contain trafficking information: studies

of the 300-kDa mannose 6-phosphate receptor. J. Biol. Chem. *269*, 12159–12166.

Dittie, A.S., Klumperman, J., and Tooze, S.A. (1999). Differential distribution of mannose-6-phosphate receptors and furin in immature secretory granules. Am. J. Cell Sci. *112*, 3955–3966.

Eaton, B.A., Haugwitz, M., Lau, D., and Moore, H.P.H. (2000). Biogenesis of regulated exocytotic carriers in neuroendocrine cells. J. Neurosci. *20*, 7334–7344.

Eipper, B.A., Park, L., Keutmann, H.T., and Mains, R.E. (1986). Amidation of joining peptide, a major pro-ACTH/endorphin-derived product peptide. J. Biol. Chem. *261*, 8686–8694.

El Meskini, R., Mains, R.E., and Eipper, B.A. (2000). Cell-type specific metabolism of endogenous PAM in rat anterior pituitary. Endocrinology *141*, 3020–3034.

Feilotter, H.E., Hannon, G.J., Ruddell, C.J., and Beach, D. (1994). Construction of an improved host strain for two hybrid screening. Nucleic Acids Res. *22*, 1502–1503.

Fricker, L.D., and Devi, L. (1993). Posttranslational processing of carboxypeptidase E, a neuropeptide-processing enzyme, in AtT-20 cells, and bovine pituitary secretory granules. J. Neurochem. *61*, 1404–1415.

Griffiths, G. (1993). Cryo and replica techniques for immunolabelling. In. Fine Structure Immunocytochemistry, ed. G. Griffiths, Berlin: Springer-Verlag, 137–203.

Hall, A. (1998). Rho GTPases and the actin cytoskeleton. Science. *279*, 509–514.

Hand, D., Perry, M.J., and Haynes, L.W. (1994). Cellular transglutaminases in neural development. Int. J. Dev. Neurosci.*11*, 709–720.

Harper, J.W., Adami, G.R., Wei, N., Keyomarsi, K., and Elledge, S.J. (1993). CDK-interacting protein Cip1 is a potent inhibitor of G1 cyclin-dependent kinases. Cell *75*, 805–816.

Hicke, L., and Riezman, H. (1996). Ubiquitination of a yeast plasma membrane receptor signals its ligand-stimulated endocytosis. Cell *84*, 277–287.

Horwitz, S.B., Shen, H.J., He, L., Dittmar, P., Neef, R., Chen, J., and Schubart, U.K. (1997). The microtubule-destabilizing activity of metaglastin (p19) is controlled by phosphorylation. J. Biol. Chem. *272*, 8129–8132.

Hughes, E.N., and August, J.T. (1981). Characterization of plasma membrane proteins identified by monoclonal antibodies. J. Biol. Chem. *256*, 664–671.

Husten, E.J., and Eipper, B.A. (1991). The membrane-bound bifunctional peptidylglycine α-amidating monooxygenase protein: exploration of its domain structure through limited proteolysis. J. Biol. Chem. *266*, 17004–17010.

Husten, E.J., Tausk, F.A., Keutmann, H.T., and Eipper, B.A. (1993). Use of endoproteases to identify catalytic domains linker regions, and functional interactions in soluble peptidylglycine α-amidating monooxygenase. J. Biol. Chem. *268*, 9709–9717.

Jones, B.G., Thomas, L., Molloy, S.S., Thulin, C.D., Fry, M.D., Walsh, K.A., and Thomas, G. (1995). Intracellular trafficking of furin is modulated by the phosphorylation state of a casein kinase II site in its cytoplasmic tail. EMBO J. *14*, 5869–5883.

Ktistakis, N.T. (1998). Signaling molecules and the regulation of intracellular transport. Bioessays *20*, 495–504.

Kuehn, M.J., and Herrmann, J.M.S.R. (1998). COPII-cargo interactions direct protein sorting into ER-derived transport vesicles. Nature *391*, 187–190.

Kuliawat, R., Klumperman, J., Ludwig, T., and Arvan, P. (1997). Differential sorting of lysosomal enzymes: out of the regulated secretory pathway in pancreatic β-cells. J. Cell Biol. *137*, 595–608.

Ladinsky, M.S., Kremer, J.R., Furcinitti, P.S., McIntosh, J.R., and Howell, K.E. (1995). HVEM tomography of the trans-Golgi network: structural insights and identification of a lace-like vesicle coat. J. Cell Biol. *127*, 29–38.

Ladinsky, M.S., Mastronarde, D.N., McIntosh, J.R., Howell, K.E., and Staehelin, L.A. (1999). Golgi structure in three dimensions: functional insights from the normal rat kidney cell. J. Cell Biol. *144*, 1135–1149.

Leung, D.W., Chen, E., and Goeddel, D.V. (1989). A method for random mutagenesis of a defined DNAsegment using a modified polymerase chain reaction. Technique *1*, 11–15.

Lorra, C., and Huttner, W.B. (1999). The mesh hypothesis of Golgi dynamics. Nature Cell Biol. *1*, E113–E115.

Mains, R.E., Alam, M.R., Johnson, R.C., Darlington, D.N., Back, N., Hand, T.A., and Eipper, B.A. (1999). Kalirin, a multifunctional PAM COOH-terminal domain interactor protein, affects cytoskeletal organization, and ACTH secretion from AtT-20 cells. J. Biol. Chem. *274*, 2929–2937.

Mains, R.E., Bloomquist, B.T., and Eipper, B.A. (1991). Manipulation of neuropeptide biosynthesis through the expression of antisense RNA for peptidylglycine α-amidating monooxygenase. Mol. Endocrinol. *5*, 187–193.

Mains, R.E., and Eipper, B.A. (1978). Coordinate synthesis of corticotropins and endorphins by mouse pituitary tumor cells. J. Biol. Chem. *253*, 651–655.

Mains, R.E., and Eipper, B.A. (1981). Coordinate, equimolar secretion of smaller peptide products derived from pro-ACTH/endorphin by mouse pituitary tumor cells. J. Cell Biol. *89*, 21–28.

Matsuuchi, L., and Kelly, R.B. (1991). Constitutive and basal secretion from the endocrine cell line, AtT-20. J. Cell Biol. *112*, 843–853.

Maucuer, A., Ozon, S., Manceau, V., Gavet, O., Lawler, S., Curmi, P., and Sobel, A. (1997). KIS is a protein kinase with an RNA recognition motif. J. Biol. Chem. *272*, 23151–23156.

Milgram, S.L., Eipper, B.A., and Mains, R.E. (1994a). Differential trafficking of soluble and integral membrane secretory granule-associated proteins. J. Cell Biol. *124*, 33–41.

Milgram, S.L., Eipper, B.A., and Mains, R.E. (1994b). Differential trafficking of soluble, and integral membrane secretory granule-associated proteins. J. Cell Biol. *124*, 33–41.

Milgram, S.L., Johnson, R.C., and Mains, R.E. (1992). Expression of individual forms of peptidylglycine alpha-amidating monooxygenase in AtT-20 cells: endoproteolytic processing and routing to secretory granules. J. Cell Biol. *117*, 717–728.

Milgram, S.L., Kho, S.T., Martin, G.V., Mains, R.E., and Eipper, B.A. (1997). Localization of integral membrane peptidylglycine? Amidating monooxygenase in neuroendocrine cells. J. Cell Sci. *110*, 695–706.

Milgram, S.L., and Mains, R.E. (1994). Differential effects of temperature. blockade on the proteolytic processing of three secretory granule-associated proteins. J Cell Sci. *107*, 737–745.

Milgram, S.L., Mains, R.E., and Eipper, B.A. (1993). COOH-terminal signals mediate the trafficking of a peptide processing enzyme in endocrine cells. J. Cell Biol. *121*, 23–35.

Milgram, S.L., Mains, R.E., and Eipper, B.A. (1996). The identification of two distinct signals responsible for the targeting of a secretory granule-associated integral membrane protein in neuroendocrine cells. J. Biol. Chem. *271*, 17526–17535.

Mironov, A.A., Weidman, P., and Luini, A. (1997). Variations on the intracellular transport theme: maturing cisternae and trafficking tubules. J. Cell Biol. *138*, 481–484.

Moore, H.P.H., and Kelly, R.B. (1986). Rerouting of a secretory protein by fusion with human growth hormone sequences. Nature *321*, 443–446.

Pahl, H.L., and Baeuerle, P.A. (1997). The ER-overload response: activation of NF-κB. Trends Biochem. Sci. *22*, 63–67.

Park, M.H., Joe, Y.A., and Kang, K.R. (1998). Deoxyhypusine synthase activity is essential for cell viability in the yeast *Saccharomyces cerevisiae*. J. Biol. Chem. *273*, 1677–1683.

Pelham, H.R.B. (2000). The Croonian lecture 1999. Intracellular membrane traffick: getting proteins sorted. Philos Trans R Soc Lond B *354*, 1471–1478.

Penzes, P., Johnson, R.C., Alam, M.R., Kambampati, V., Mains, R.E., and Eipper, B.A. (2000). An isoform of kalirin, a brain-SPecific GDP-GTP exchange factor, is enriched in the post-synaptic density fraction. J. Biol. Chem. *275*, 6395–6403.

Raska, I., Pliss, A., Mandys, V., Risueno, M.C., and Lojda, Z. (1998). Processing of free cells for electron microscopy using a fibrin clot. Acta Histochem. *100*, 309–313.

Ratovitski, E.A., Alam, M.R., Quick, R.A., McMilan, A., Bao, C., Kozlovsky, C., Hand, T.A., Johnson, R.C., Mains, R.E., Eipper, B.A., Lowenstein, C.J. (1999). Kalirin inhibition of inducible nitric-oxide synthase. J. Biol. Chem. *274*, 993–999.

Robinson, M.S. (1997). Coats and vesicle budding. Trends Cell Biol. *7*, 99–102.

Roth, A.F., and Davis, N.G. (1996). Ubiquitination of the yeast a-factor receptor. J. Cell Biol. *134*, 661–674.

Schmid, S., and Damke, H. (1995). Coated vesicles: a diversity of form and function. FASEB J. *9*, 1445–1453.

Schmid, S.L. (1997). Clathrin-coated vesicle formation and protein sorting: an integrated process. Annu. Rev. Biochem. *66*, 511–548.

Schnabel, E., Mains, R.E., and Farquhar, M.G. (1989). Proteolytic processing of pro-ACTH/endorphin begins in the Golgi complex of pituitary corticotropes and AtT-20 cells. Mol. Endocrinol. *3*, 1223–1235.

Shamu, C.E. (1997). Signal transduction: splicing together the unfolded-protein response. Curr. Biol *7*, 67–70.

Steveson, T.C., Keutmann, H.T., Mains, R.E., and Eipper, B.A. (1999). Phosphorylation of cytosolic domain Ser^{937} affects both biosynthetic and endocytic trafficking of peptidylglycine α-amidating monooxygenase. J. Biol. Chem. *274*, 21128–21138.

Tausk, F.A., Milgram, S.L., Mains, R.E., and Eipper, B.A. (1992). Expression of a peptide processing enzyme in cultured cells: truncation mutants reveal a routing domain. Mol. Endocrinol. *6*, 2185–2196.

Thornalley, P.J. (1998). Glutathione-dependent detoxification of alpha-oxoaldehydes by the glyoxalase system. Chem. Biol. Interact. *111*, 137–151.

Tooze, J., Hollinshead, M., Fuller, S.D., Tooze, S.A., and Huttner, W.B. (1989). Morphological and biochemical evidence showing neuronal properties in AtT-20 cells and their growth cones. Eur. J. Cell Biol. *49*, 259–273.

Tooze, J., and Tooze, S.A. (1986). Clathrin-coated vesicular transport of secretory proteins during the formation of ACTH-containing secretory granules in AtT20 cells. J Cell Biol. *103*, 839–850.

Tooze, S.A. (1998). Biogenesis of secretory granules in the trans-Golgi network of neuroendocrine and endocrine cells. Biochim. Biophys. Acta *1404*, 231–244.

Urbe, S., Tooze, S.A., and Barr, F.A. (1997). Formation of secretory vesicles in the biosynthetic pathway. Biochim. Biophys. Acta *1358*, 6–22.

Varlamov, O., Eng, F.J., Novikova, E.G., and Fricker, L.D. (1999). Localization of metallocarboxypeptidase D in AtT-20 cells. J. Biol. Chem. *274*, 14759–14767.

Wan, L., Molloy, S.S., Thomas, L., Liu, G., Xiang, Y., Rybak, S.L., and Thomas, G. (1998). PACS-1 defines a novel gene family of cytosolic sorting proteins required for trans-Golgi network localization. Cell *94*, 205–216.

Wold, F. (1981). In vivo chemical modification of proteins. Annu. Rev. Biochem. *50*, 783–814.

Yun, H.-Y., Milgram, S.L., Keutmann, H.T., and Eipper, B.A. (1995). Phosphorylation of the cytosolic domain of peptidylglycine α-amidating monooxygenase. J. Biol. Chem. *270*, 30075–30083.

Zhou, A., Bloomquist, B.T., and Mains, R.E. (1993). The prohormone convertases PC1 and PC2 mediate distinct endoproteolytic cleavages in a strict temporal order during POMC biosynthetic processing. J. Biol. Chem. *268*, 1763–1769.

Zhou, A., and Mains, R.E. (1994). Endoproteolytic processing of POMC and the peptide biosynthetic endoproteases PC1 and PC2 in neuroendocrine cells overexpressing PC1 or PC2. J. Biol. Chem. *269*, 17440–17447.